

AD-A139 357

FRACTURE MECHANICS OF SUBLAMINATE CRACKS IN COMPOSITE
LAMINATES(U) DREXEL UNIV PHILADELPHIA PA DEPT OF
MECHANICAL ENGINEERING AN. . A S WANG FEB 83

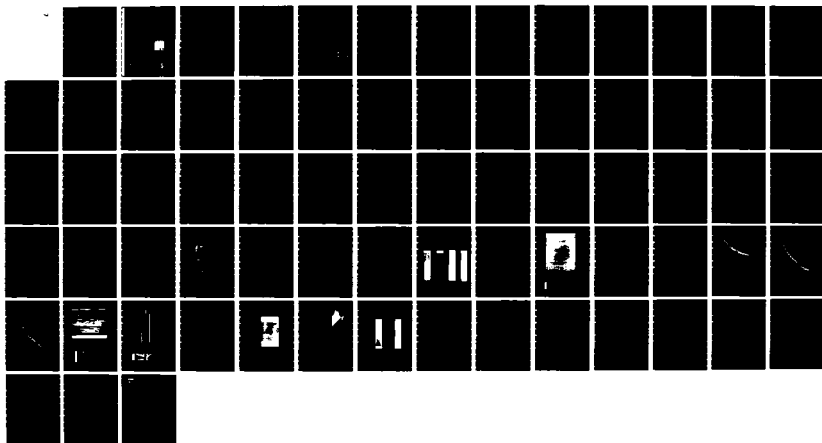
1/1

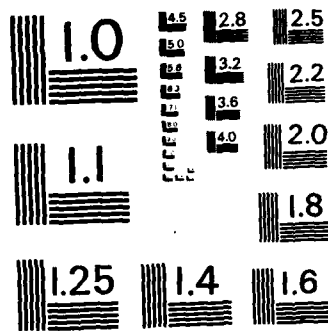
UNCLASSIFIED

AFOSR-TR-84-0168 F49620-79-C-0206

F/G 11/4

NL





MICROCOPY RESOLUTION TEST CHART
NATIONAL BUREAU OF STANDARDS - 1963 - A

3

AD A 1 3 9 3 5 7

FRACTURE MECHANICS OF SUBLAMINATE CRACKS
IN COMPOSITE LAMINATES*

DTIC FILE COPY



College of Engineering
Department of
Mechanical Engineering
and Mechanics
Philadelphia, PA 19104

(215) 895-2352-53

DTIC
ELECTRONIC
S MAR 23 1984
A

Approved for public release;
distribution unlimited.

84 03 22 119

| REPORT DOCUMENTATION PAGE | | READ INSTRUCTIONS BEFORE COMPLETING FORM |
|---|--|---|
| 1. REPORT NUMBER AFOSR-TR-84-0168 | 2. GOVT ACCESSION NO. AD A139357 | 3. RECIPIENT'S CATALOG NUMBER |
| 4. TITLE (and Subtitle) FRACTURE MECHANICS OF SUBLAMINATE CRACKS IN COMPOSITE LAMINATES | | 5. TYPE OF REPORT & PERIOD COVERED INTERIM REPORT Oct. 1982 - Feb. 1983 |
| | | 6. PERFORMING ORG. REPORT NUMBER |
| 7. AUTHOR(s) A. S. D. Wang | | 8. CONTRACT OR GRANT NUMBER(s) F49620-79-C-0206 |
| 9. PERFORMING ORGANIZATION NAME AND ADDRESS DREXEL UNIVERSITY DEPT OF MECHANICAL ENGINEERING PHILADELPHIA, PA 19104 | | 10. PROGRAM ELEMENT, PROJECT, TASK AREA & WORK UNIT NUMBERS 61102F 2307/B2 |
| 11. CONTROLLING OFFICE NAME AND ADDRESS AIR FORCE OFFICE OF SCIENTIFIC RESEARCH/NA BOLLING AFB DC 20332 | | 12. REPORT DATE February 1983 |
| | | 13. NUMBER OF PAGES 67 |
| 14. MONITORING AGENCY NAME & ADDRESS (if different from Controlling Office) | | 15. SECURITY CLASS. (of this report) UNCLASSIFIED |
| | | 15a. DECLASSIFICATION/DOWNGRADING SCHEDULE |
| 16. DISTRIBUTION STATEMENT (of this Report) Approved for public release; distribution unlimited. | | |
| 17. DISTRIBUTION STATEMENT (of the abstract entered in Block 20, if different from Report) | | |
| 18. SUPPLEMENTARY NOTES Presented at the AGARD Structural and Materials Specialists Meetings. April 10-15, 1983. London, United Kingdom. | | |
| 19. KEY WORDS (Continue on reverse side if necessary and identify by block number) Fracture mechanics, transverse cracks, delamination, mechanistic modelling, probabilistic simulation, sub-laminate cracking interactions, influence on final failure mechanisms | | |
| 20. ABSTRACT (Continue on reverse side if necessary and identify by block number) This paper presents an overview of a fracture mechanics approach to some of the most frequently encountered matrix-dominated, sub-laminate cracks in epoxy-based composite laminates. By "sub-laminate", it is meant that the cracks are internal to the laminate, generally invisible macroscopically; but are much larger in size than those microcracks considered in the realm of micromechanics. The origin of sub-laminate cracks is assumed to stem from the coalescence of natural material flaws (also microcracks), which occur | | |

under a certain favorable laminate stress condition. Thus, the mechanisms of sub-laminate crack initiation and propagation are modelled by a mechanistic/probabilistic formulation. Specific results from several analytical/experimental investigations using graphite-epoxy laminates are presented and discussed.

FRACTURE MECHANICS OF SUBLAMINATE CRACKS
IN COMPOSITE LAMINATES*

A. S. D. Wang
Drexel University
Department of Mechanical Engineering
Philadelphia, PA 19104

February, 1983

DTIC
ELECTE
MAR 23 1984
A

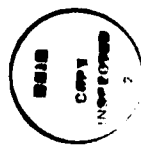
* Paper delivered at the AGARD Structural and
Materials Specialists Meetings. April 10 - 15,
1983. London, United Kingdom.

AIR FORCE... (AFSC)
NOTICE...
This te... is
approved... IAW APR 190-12.
Distribution... limited.
MATTHEW J. KEAPER
Chief, Technical Information Division

ABSTRACT

This paper presents an overview of a fracture mechanics approach to some of the most frequently encountered matrix-dominated, sub-laminate cracks in epoxy-based composite laminates. By "sub-laminate", it is meant that the cracks are internal to the laminate, generally invisible macroscopically; but are much larger in size than those microcracks considered in the realm of micromechanics. The origin of sub-laminate cracks is assumed to stem from the coalescence of natural material flaws (also microcracks) which occur under a certain favorable laminate stress condition. Thus, the modelling of the mechanisms of sub-laminate crack initiation and propagation is essentially mechanistic and probabilistic in nature. Some specific results from several analytical/experimental investigations using graphite-epoxy laminates are presented and discussed in this paper.

- 1 -



| | |
|--------------------|-------------------------------------|
| Accession For | |
| NTIS GRA&I | <input checked="" type="checkbox"/> |
| DTIC TAB | <input type="checkbox"/> |
| Unannounced | <input type="checkbox"/> |
| Justification | |
| Distribution/ | |
| Availability Codes | |
| Special | |

AI

INTRODUCTION

Failure mechanisms in structural composite laminates have been viewed at several dimensional levels. Consider, for instance, the curved laminated panel shown in Figure 1(a). Failure of this structural component may be caused by a loss of the global stiffness when the applied load reaches a certain critical value. To describe analytically the associated failure mechanisms and hence to determine the critical load, structural mechanics methods such as buckling and post-buckling theories are employed, which relate the change of the structural geometry to the applied load. In this type of analysis, the stiffness of the laminated panel and the kinematics of its displacements are among the most predominant factors.

On the other hand, the same panel may fail due to a loss of strength at a local defect; for example, at a bolt-hole, Figure 1(b). In this case, rupture of material will begin at the hole and may propagate into a large crack whenever a certain load condition is reached. But in order to define the conditions for rupture initiation and propagation, a knowledge of the actual stress field around the hole, and the physical mechanisms of the material rupture process is essential. To this end, it will be necessary to focus further on the local defect area at a much smaller dimensional level. As illustrated in Figure 1(c), for instance, the lamination details of the panel, such as layer interfaces and the stacking sequence are now identifiable. Consequently, quantities of size comparable to the layer thickness become important; the influence of an interface defect (i.e. delamination), a translaminar crack, a fiber split, etc. are new factors to be considered. For it is believed that the development of rupture around the hole is precipitated by these sub-laminate cracking activities,

any failure analysis performed at this dimensional level must first address the individual mechanisms of the various sub-laminate cracks, and, then their interaction and coalescence mechanisms when they occur simultaneously and/or sequentially.

It is well known that the formation and propagation mechanisms of a crack are governed by the conditions that exist in the close vicinity of the crack front. In the case of the sub-laminate cracks mentioned above, further focusing of the crack front region will reveal the microstructure of the composite system, Figure 1(d). Here, a clear distinction can be made between the fiber and the matrix phases of the material. At this dimensional scale, one also finds a random distribution of material microflaws, be it voids, broken fibers, matrix crack, debonded fiber-matrix interfaces, just to mention a few, see Figure 1(e).

Although the inherent microflaws are small in size, usually on the order of the fiber diameter, they may behave as local stress risers under the applied load. When a certain local condition is reached, the microflaws interact and coalesce to form an actual crack, much larger in size, and identifiable at the sub-laminate level. Hence, a proper analysis of the mechanisms must be capable of delineating the individual behavior of the various types of stress risers, and their interactions when one is located close to another. All these depend profoundly on the probabilistic nature of the microflaws in terms of their size, location and density distributions.

The physical process of material failure as portrayed in the preceding discussions is seen to span a wide range of dimensions. Though the entire process is essentially one continuous event, failure analysis could

be conducted only within isolated dimensional regimes. As illustrated in Figure 1, the entire dimensional spectrum is separated roughly into three analysis regimes; namely the structural mechanics, the macromechanics and the micromechanics regimes. Within each analysis regime, the material failure process involves a distinct set of material and geometrical parameters.

Analytical and experimental treatments on laminate failure at the structural mechanics level have generally been approached, using the classical lamination theory (see [1]). Stiffness-predominant structural responses such as panel buckling and post-buckling have been successfully analyzed [2]. The effect of local material damage (e.g. from a bolt-hole, a delamination caused by impact, etc.) upon the global response can also be evaluated [3]. But, a more detailed description about the damage formation and propagation mechanisms always required separate treatment.

For a class of epoxy-based composite laminates, e.g. graphite-epoxy systems, material damage mechanisms around a bolt-hole or near the tip of a line-notch have been modeled by the crack growth formula that are derived from the classical fracture mechanics for structural metals [4-6]. Essentially, the notched laminate is regarded as a 2-dimensional body, and the crack growth from the notch is assumed self-similar and catastrophic. In order for the fracture formula to correlate with a body of experimental data, the notch size parameter must be adjusted to include an empirically defined "intense energy region" at the crack tip. Thus, together with the laminate's fracture toughness (K_c or G_c), yet to be determined experimentally, the model consists of two disposable parameters which must be adjusted to fit a given set of test data.

Clearly, the empiricism in this approach is less than desirable. As was discussed earlier, the development of material damage, say around a small bolt-hole, is precipitated by a multitude of sub-laminate cracking activities in that region. The term "intense energy region" is in fact a gross representation of these activities at a larger dimensional scale. It would be ideal, therefore, to carry the analysis across the dimensional boundary into the macromechanics regime (see Figure 1), so as to understand how sub-laminate crackings lead to the damage development around the hole.

Early studies on fibrous composites dealt mostly failure mechanisms in the micromechanics regime. For instance, a considerable amount of theoretical and experimental treatments was given on the subject of the fiber-matrix interface mechanics [7 - 10]. Fracture models for various microcracks such as depicted in Figure 1(e) are characterized in terms of energy absorption processes, including interface debonding, fiber pull-out, matrix crack bridging [11], etc. Although the modeling of these various microflaws is basic to the strengthening mechanisms of the composite system at the fiber-matrix level, it remains to incorporate these "micro" models into some analysis which includes the mutual interaction and the coalescence mechanisms of the microflaws. Indeed, it would be ideal, again, to have a fracture model which accounts for both the mechanistic failure behavior of the microflaws and the probabilistic nature of their existence; the analysis can then be carried into the regime of macromechanics.

Several mechanistic/probabilistic failure models have been attempted in the past. Zweben and Rosen [12] studied, for example, the tensile strength characteristics of unidirectional composites, assuming the micro-

flaws a distribution of local broken fibers. The basic concept can be extended to multi-directional laminated systems, but the complexity in geometry as well as the multiplicity of failure modes make this type of effort so far unproductive.

In recent years, increased attention has been given to fracture modeling within the general confines of macromechanics, as illustrated in Figure 1(c). At this analysis level, the individual material layers in the laminate are approximated as being homogeneous and anisotropic, where no distinction of the fiber and the matrix phases need be made. Essentially, the stiffness properties of the material layer are represented by some "effective" values characterized experimentally as basic material constants, but failure in the material layer is not governed by a set of strength constants. Rather, it is determined by a certain fracture event which occurs at the "sub-laminate" level. Since by a homogeneous approximation the identity of the inherent material microflaws also becomes lost, only their gross effects upon the formation and propagation of sub-laminate cracks can be retained. Thus, an empirically defined "effective" crack size is introduced.

As it will be discussed in detail later in this paper, the macroscopic view point allows a rational formulation for a general fracture model for a class of sub-laminate cracking in epoxy-based composite laminates. Early studies, notably by Corten [13], Wu [14], Kanninen, et. al. [15], have articulated the viability of such an approach. Major advances have since been made, due mainly to the ever-expanding computational capabilities and ever-revealing NDT methods. These modern facilities have provided a means for a more rational correlation between experiments and analysis.

In a series of papers [16 - 22], Wang, Crossman, et. al. developed a unified energy model within the context of macromechanics. It describes the growth mechanisms in a class of matrix-predominant sub-laminate cracks. The specific cracks considered included interlaminar (delamination) and translaminar (fiber-split) crackings, found most prevalent in graphite-epoxy laminates.

This paper is a summary of their major findings obtained during the course of several analytical and experimental investigations

FRACTURE CONSIDERATIONS IN MACROMECHANICS

The energy model developed by Wang and Crossman is formulated on the energy release rate concept of the linear elastic fracture mechanics (LEFM). All variables in the model are defined within the context of the macromechanics. Since fibrous composites possess some unique characteristics, special considerations had to be given to defining some of the variables.

Application of the Griffith Criterion

The essence of the LEFM is that material failure is not defined from the stand-point of strength as a constant material property. Rather, it is determined by an analysis of the kinetics of the actual process of fracture propagation. The classical result of Griffith [23] pertained to an elastic plate which is uniformly stretched in one direction by σ . The plate has a through crack of size $2a$, orientated normal to the direction of σ . The length of the crack is assumed small but finite; and, the material is homogeneous and isotropic. Griffith postulated that at the instance of crack extension, a loss of the stored elastic strain energy near the crack-tip region is resulted; this energy is converted into the

surface energy of the crack. A balance of energy during a virtual crack extension leads to the criterion

$$\frac{\partial U}{\partial a} = \frac{\partial S}{\partial a} \quad (1)$$

Equation (1) defines the general condition under which the existing crack begins to propagate in self-similar mode.

For the plate problem, the critical stress at the instance of crack extension can be derived from (1), giving

$$\sigma_c = \left(\frac{2E\gamma}{\pi a}\right)^{1/2} \quad (2)$$

where γ is the free surface energy density of the material.

When applied to engineering problems, the Griffith theory is often modified for practical considerations. For instance, Equation (2) becomes unbounded as $a \rightarrow 0$. Certainly, no real material can sustain an infinite stress. This limitation, however, can be circumvented by invoking the existence of material flaws. That is to assume for the material some characteristic distribution of flaws; the worst of which, having a size of $2a_0$, acts like a real crack. It then determines a finite critical stress according to Equation (2).

Of course, flaws do exist in real materials, especially in fibrous composite systems. But the physical identity is lost at the dimensional level where the analysis is performed. The quantity a_0 can be defined only empirically as an intrinsic material property. As it will be discussed later, the value of a_0 can be orders of magnitude larger than the fiber diameter in, say, graphite-epoxy systems.

Another practical consideration is related to the definition of γ , the free surface energy density of the material. For crack in brittle material such as glass, then γ is as defined. For most other engineering materials, crack extension is found to associate a certain degree of inelastic deformation near the crack-tip region. Furthermore, the crack extension path, or the crack surface, shows a certain degree of ruggedness, depending on the heterogeneity of the material viewed at a micro-scale. Early studies by Irwin [24], Orowan [25] and others on structural metals considered the right-hand side of Equation (1) the irreversible work required to create a unit crack surface area. Hence, the quantity γ can be interpreted as the energy dissipated in the crack-tip region during crack extension. Clearly, γ will then depend on the inelasticity as well as the microscopic heterogeneity of the material locally (near the crack-tip). It, therefore, must also be regarded as an intrinsic property of the material to be defined at the macromechanics level. Conceivably, γ has to be an averaged value over a relatively large crack surface area for fibrous composites in order for it to be a material constant.

These considerations are of fundamental importance when a crack-like failure is modeled at the macroscopic dimensional level. For only in this context can a macroscopic fracture model be developed along the rational arguments of the classical fracture mechanics.

In common practice, the right-hand side of Equation (1) is replaced by $G_c (= 2\gamma)$, known as the critical energy release rate of the material. The left-hand side is a function of the applied load, the geometry of the body and the size of the crack. Thus, for a crack undergoing self-similar extension, the Griffith criterion is expressed as

$$G(\sigma, a) = G_c \quad (3)$$

Accordingly, the development of the fracture model for sub-laminate cracks rests upon the calculation of $G(\sigma, a)$ and the physical measurement of G_c . The latter is simply a material constant.

The Calculation of $G(\sigma, a)$

In the theory of the LEFM, the singular stress field near a crack tip in a homogeneous, isotropic elastic body is represented by analytical functions in the theory of complex variables [26]. The near-field stresses are obtained for three particular modes of the crack opening. These are known as the opening mode (I), the sliding mode (II) and the anti-plane shearing mode (III). For each mode, the stresses are expressed in terms of the associated stress intensity factor K [27]; and consequently, the associated $G(\sigma, a)$ is computed in terms of K . Since the relation between K and G is one-to-one, Equation (3) reduces to the form

$$K(\sigma, a) = K_c \quad (4)$$

Similar relations between K and G for orthotropic media having a crack orientated along one of the major axes can also be obtained [28]. But the analytical solutions for the singular stress field often require tedious mathematical derivations.

Direct solution methods for $G(\sigma, a)$ have been available; among them are the well-known J-integral method [29, 30] and the method of virtual crack closure technique by Irwin [31].

Irwin [31] observed that the elastic strain energy released during a virtual crack extension Δa is equal to the work done in closing it again. The inverse problem provides the solution for the surface tractions $\bar{\sigma}$

over Δa . The crack-tip energy release rate is then represented by

$$G = \lim_{\Delta a \rightarrow 0} \frac{1}{2\Delta a} \int_0^{\Delta a} (\bar{\sigma} \cdot \Delta \bar{u}) da \quad (5)$$

where $\Delta \bar{u}$ is the crack opening displacement vector over Δa .

If the crack extension involves all three modes (I, II, III), the vector product in Equation (5) will give a sum of three scalars, associated respectively with G_I , G_{II} , and G_{III} .

The virtual crack-closure representation is particularly adaptive to machine computations. Rybicki and Kanninen [32] suggested a 2-dimensional finite element technique to evaluate G for a line crack in a plane. The crack-tip stress vector $\bar{\sigma}$ and the displacement vector $\Delta \bar{u}$ in Equation (5) are approximated by the nodal forces and displacements respectively, in a finite element representation (for detail, see [18]).

Wang and Crossman applied this technique in a generalized plane strain finite element routine [33], which can simulate a line crack propagation in the 2-dimensional cross-section of a laminate. Since a general laminate under load may suffer cross-sectional warping, the routine actually computes 3-dimensional stresses and displacements [33].

If a laminate is subjected to the far-field stress σ_0 and a sub-laminate crack is to be simulated, the crack-tip energy release rate can be expressed in the general form

$$G_e = C_e (a/t) \cdot t \cdot (\sigma_0/E_0)^2 \quad (6)$$

where E_0 is laminate stiffness in σ_0 direction, and t is the linear scale between the actual model and the finite element model. C_e is a function dependent only on the crack size a , which is routinely generated for a

given type of crack in a given laminate.

Similarly, if the laminate is subjected to a uniform temperature load ΔT , and if a thermally induced crack opening is resulted, then the associated energy release rate at the crack tip is expressed by

$$G_T = C_T(a/t) \cdot t \cdot (\Delta T)^2 \quad (7)$$

Generally, the laminate is prestressed by a $-\Delta T$ due to curing, so a combined effect is resulted when σ_o is applied;

$$G = [(C_e)^{1/2} \cdot e_o + (C_T)^{1/2} \cdot \Delta T]^2 \cdot t \quad (8)$$

where e_o is the far-field strain ($= \sigma_o/E_o$).

It is seen that the finite element technique is extremely versatile, and can be efficiently executed for simulating complicated sub-laminate crackings such as delamination.

Nonetheless, the accuracy of the technique has been a subject of concern of many analysts, because of its approximate nature in representing a mathematically singular stress field. As has been demonstrated by Raju and Crews [34], Spilker and Chou [35], and Wang and Choi [36], the finite element stress solutions could lose significant accuracy in the small vicinity of the singular point; the region in which the stress becomes inaccurate is generally much smaller than, say, a fiber diameter, due to the very nature of the singularity [36]. However, it can also be demonstrated that the stresses in that small region do not contribute significantly to the crack opening energy release rate, especially for a crack size much larger in proportion.

Figure 2 shows a close comparison between the finite element computed G and the elasticity solution counter-part, for a transverse crack located in the mid-layer of a 3-layer laminate (see insert of Figure 2). The extreme layers are designated as material 1 and the mid-layer as material 2. Both had to be assumed elastic isotropic materials. The exact solution for G as a function of the crack size a is given by Isida [37], using complex stress potentials; while the finite element solution is computed using a rather coarse constant-strain, triangular element mesh. It is seen that the finite element solution for $G(a)$ compares well with the exact solution. To obtain accurate stress closest to the crack tip, one can still resort to the finite element method using either a finer mesh or a higher-order element formulation [38]. But, such extreme measures are often unnecessary for the computation of G .

The Evaluation of G_c

When fracture occurs in the material, the energy released in the process is expected to depend on the morphology of the fracture surface, which must be examined at the microscale. Fibrous composites are known to possess complex fracture surface details, even in matrix-predominant cracks. The observed delamination surfaces in graphite-epoxy composites show, for instance, a considerable raggedness because the crack must pass around the reinforcing fibers. But, at the macroscopic level, the crack surface details are "smoothed out"; and their effects are reflected in the measured quantity of the fracture resistance G_c .

For this reason, G_c measured for some matrix-predominant fractures in epoxy-based composites has been found to depend on the direction of fracture propagation. Cullen [39] and Williams [40] considered two different

cases of delamination as illustrated in Figure 3. The first case is $0^\circ/0^\circ$ delamination in which the crack path is in the fiber direction, while the second is $90^\circ/90^\circ$ delamination where the crack path is transverse to the fiber direction. The experiments were performed using a graphite-epoxy unidirectional laminate, subjected to mode-I cracking condition. They found that the microscopic morphology of the $90^\circ/90^\circ$ delamination surface exhibited considerably more raggedness than the $0^\circ/0^\circ$ delamination surface. This resulted in marked differences for the measured G_c . Note that these two fracture events occur essentially in the same interface when viewed macroscopically. Yet, the respective G_c values can differ greatly depending on the direction of the crack propagation.

Hence, when the Griffith formula (3) is applied for cracks in composites, the term G_c requires a precise qualification. Similarly, when a test method is devised to measure G_c , it is also necessary to consider the dimensional and directional characteristics of the measured data.

Mode-I interlaminar G_{Ic} . A commonly used test method to determine interlaminar G_{Ic} is the splitting cantiliver beam. Cullen [39] and Wilkins [41] have used this method to determine the interlaminar G_{Ic} when the crack is propagating in the direction of the fibers ($0^\circ/0^\circ$ delamination). For some graphite-epoxy systems, they found that G_{Ic} at room temperature is about 0.85 lb/in, or 130 J/m^2 . This value is about twice the G_{Ic} measured for pure epoxy resin. Williams [40] used a compact specimen which simulates roughly a $90^\circ/90^\circ$ delamination. He found, for the same material system, a G_{Ic} value of 1.3 lb/in, about three times that of the pure resin. Williams explained that the fracture surface in his specimens showed fiber breakage as well as fractured epoxy debris; this had resulted in a higher value for G_{Ic} than that found for $0^\circ/0^\circ$ delamination by Cullen [39].

In another paper by Wilkins, et. al. [42], it is reported that G_{Ic} in delamination of $0^\circ/90^\circ$ interface is also higher than that of $0^\circ/0^\circ$ delamination. These findings reaffirm the directional dependent nature of G_{Ic} .

Mixed-mode interlaminar $G_{(I, II)c}$. The splitting cantiliver beam method has also been used in mixed-mode cracking experiment. In this case, it is necessary to apply different loads at the top and the bottom parts of the split so as to create both an opening (I) and a sliding (II) action. Vanderkley [43] and Wilkins [41] conducted tests on the same graphite-epoxy system (used for their mode-I tests), and found the total energy release rate $G_{(I, II)c} = G_{Ic} + G_{IIc}$ which exhibited a strong dependence on the G_{II}/G_I ratio.

This phenomenon is not uncommon in mixed-mode fracture. Similar observations were reported for brittle metals as well as pure epoxy resins [44]. It is, perhaps, more pronounced in fibrous composites. Generally, it is thought that the increased fracture resistance is the result of excessive matrix yielding under shear, as well as crack-closure friction due to the sliding action.

In an experiment on double-notched off-axis unidirectional graphite-epoxy laminates, Wang, et. al. [45] measured the mixed-mode $G_{(I, II)c}$ as a continuous function of G_{II}/G_I , see Figure 4. It is seen that $G_{(I, II)c}$ is monotonically increasing with G_{II}/G_I .

But in the same experiment, it shows also that the opening part G_{Ic} remains roughly independent of G_{II}/G_I . This suggests that mixed-mode crack is essentially controlled by mode-I. Of course, such a suggestion is only temporary; more study is needed to fully understand the true nature of the mixed-mode crack mechanisms.

MECHANICS OF TRANSVERSE CRACKS

Physical Mechanisms at the Macroscale

Transverse cracks are found in epoxy-based laminates, even at a low loading level. When viewed at the macroscopic scale, the cracking action is simply a sudden separation of fibers by breaking the epoxy bond. To illustrate, consider as an example a $[0/90]_s$ type laminate such as shown by the insert in Figure 2. There, material 1 is the 0° -layer and material 2 is the 90° -layer. Under the far-field tensile load, material 2 could suffer multiple transverse cracks. Generally, the sequence of events is as follows: A single crack forms first when the applied load reaches a certain critical value, which defines the "onset" of the events; as the applied load increases, more similar cracks are formed. If there is no other failure mode setting in at high load (e.g. 0° -rupture, delamination, etc.), the number of transverse cracks will continue increasing, until it reaches a saturation density.

Figure 5 shows a load-sequence x-radiographs taken for a $[0/90]_s$ graphite-epoxy laminate under ascending tensile load. Transverse cracks in the 90° -layer are seen to form in increasing numbers. From these photographs, a plot of crack density (e.g. cracks per inch of specimen length) versus the applied load can be obtained. Figure 6 shows a family of such experimental plots for a series of $[0/90_n/0]$ laminates, $n = 1, 2, 3, 4$.

Examination of the plots in Figure 6 reveals several interesting features. First, the onset load for the first transverse crack seems to be influenced profoundly by the 90° -layer thickness, especially when it is very thin. Take, for example, the case of $n = 1$ in Figure 6, the onset load is almost twice that of $n = 2$.

Secondly, the crack density also shows dependence on the same thickness factor. Generally, the laminate with thinner 90°-layer is capable of yielding a higher crack density. But, for the case of $n = 1$, failure of 0°-layer at high load interrupted the development of more transverse cracks.

The 90°-layer thickness effect on transverse cracking was first documented experimentally by Bader, et. al. [46]. They attributed the effect to the constraining actions of the adjacent 0°-layers. Observing that a transverse crack can be no larger than the 90°-layer thickness, the energy release rate which drives the crack is thus limited by the same factor. It is the total strain energy trapped in the 90°-layer which determines the onset of the cracking, not the in-situ tensile stress.

As for the effect on crack density, it has been explained by the existence of a "shear-lag" zone at the transverse crack root [46 - 48]. That is an interlaminar shear stress is developed on the 0/90 interface where a transverse crack terminates. This shear stress is singular at the crack root, but decays exponentially a distance away [20]. Similarly, the in-situ tensile stress in the 90°-layer is nil at the transverse crack, but it regains its far-field value outside the shear-lag zone. Thus, ideally, any two adjacent cracks should be spaced by the shear-lag distance. Since this distance is proportional to the 90°-layer thickness [20], hence the observed thickness effect on crack density.

Although the shear-lag concept is ideally correct, the so-called "characteristic" spacing of transverse cracks does not occur in practice. Often, transverse cracking leads to other failure modes, and/or vice versa [21].

At the microscopic level, the mechanisms of a transverse crack are much more perplexed. For example, the exact kinematics of crack formation is not fully known. Post-test SEM examination of the crack surfaces generally gives a very ragged appearance; tiny epoxy debris and sometimes broken fibers are also seen [40]. Figure 7 shows an x-ray plane view of a $[\underline{+25/90}_2]_s$ laminate after transverse cracking, left, and an edge-view micrograph on the right. It is seen that the transverse crack is practically a plane crack of a rectangular dimension, which is bounded by the width of the specimen and the 90° -layer thickness. There is no evidence to indicate that the crack formation is progressive in nature. In fact, all experiments tend to suggest a sudden dynamical formation.

This dynamical nature, though still conjectured, has been qualified by many who monitored the acoustics emitted during the crack formation (see, e.g. [49]).

While it is difficult to reduce these physically observed facts into a general law, they nevertheless provide the necessary rational for the formation of an analytical model. In what follows, an energy formulation is presented, which describes the most essential observed characteristics of the transverse cracking phenomenon.

The Energy Formulation

For purpose of clarity, consider a $[0/90]_s$ type laminate, as shown in Figure 8. It will be assumed that, in the 90° -layer, the material has a random distribution of microflaws. The gross effects of the microflaws at the macroscopic scale are represented by a characteristic distribution of "effective" flaws which cannot be physically seen. But, under stress, these effective flaws are capable of propagating suddenly into transverse

cracks, which are physically real. The individual size of the effective flaws is denoted by $2a$; and any two adjacent flaws are spaced by a distance S , see Figure 8.

Given a unit length of the specimen, there is a probability density function $f(a)$, and a probability density function $f(S)$. For sake of no evidence to suggest otherwise, the two functions are assumed to take a form for normal distributions [50];

$$f(a) = \frac{1}{a\sqrt{2\pi}} \exp \left[-(a - \mu_a)^2 / 2\sigma_a^2 \right] \quad (9)$$

$$f(S) = \frac{1}{S\sqrt{2\pi}} \exp \left[-(S - \mu_s)^2 / 2\sigma_s^2 \right] \quad (10)$$

where μ and σ are the mean and the standard deviation of the respective distribution functions.

Among the effective flaws, the size of the "worst" one is denoted by $2a_0$. For definiteness, assume a_0 the 99 percentile of $f(a)$. That is 99% of the flaws are smaller than $2a_0$.

Then, under the far-field load, say e_0 , the "worst" flaw $2a_0$ will become the first transverse crack. The critical value for e_0 at the onset is calculated by substituting Equation (8) into the Griffith criterion (3):

$$\left[(C_e)^{1/2} \cdot e_0 + (C_T)^{1/2} \cdot \Delta T \right]^2 \cdot t = G_c \quad (11)$$

where C_e and C_T are evaluated at $a = a_0$.

As has been detailed earlier, the energy release rate coefficients C_e and C_T are generated numerically by the finite element crack-closure routine, given the geometry and material moduli of the laminas. Thus, in Equation (11), all quantities except e_0 will be given: ΔT is the tem-

perature load due to cooling; t is the linear scale between the finite element model and the actual model; and G_c takes the value of G_{Ic} which is measured for mode-I $90^\circ/90^\circ$ delamination.

Now, the difficulty rests upon the choice of a_0 , or for the same matter, the choice of μ_a and σ_a in the distribution function (9).

Clearly, $2a_0$ must be smaller than the 90° -layer. But the latter can be made arbitrarily large. Hence, a finite bound on a_0 exists even if the 90° -layer thickness is unbounded.

As an example, consider the experimental results reported in [21]. The tensile strength of T300/934 [90_g] laminates averaged $\sigma_u \sim 7000$ psi. If the same "effective" flaw concept is assumed, then the "worst" flaw in the laminate (parallel to fibers) determines the strength according to the Griffith formula (2), yielding

$$a_0 = G_c E / \pi \sigma_u^2 \quad (12)$$

with $E = 1.7 \times 10^6$ psi and $G_c = 0.9$ lb/in for $0^\circ/0^\circ$ mode-I delamination, Equation (12) determines $a_0 \sim 0.01$ ", or about 2 times the ply thickness of the T300/934 systems.

It may be assumed that for the $90^\circ/90^\circ$ mode-I delamination in an unbounded 90° -layer, the "worst" effective flaw size should be no greater than $a_0 \sim 0.01$ ". Indeed, in several experimental correlations conducted by Wang and Crossman [19, 20, 21], using the same material system, a_0 is found in the order of 0.0075 ", or 1.5 times the ply thickness.

Numerical Examples by Monte-Carlo Simulation

In what follows, the transverse cracking phenomenon will be simulated numerically by the so-called Monte-Carlo random search technique. The

considered laminates are in the form $[0_2/90_n]_s$, $n = 1, 2$ and 3 . The material system is the AS-3501-06 graphite-epoxy system (for the material moduli, see [51]). The nominal ply thickness of this system is $0.0052''$.

In order to define the parameters μ and σ in the $f(a)$ and $f(S)$ distribution functions, the following values are chosen for the laminates $n = 2$ and 3 :

$$\mu_a = 0.0036'', \sigma_a = 0.0013'' \quad (13)$$

$$\mu_s = 0.0125'', \sigma_s = 0.0046'' \quad (14)$$

These are chosen to reflect the fact that a_o , being over 99% of $f(a)$, may take a value (see [50]),

$$a_o = \mu_a + 3\sigma_a = 0.0075'' \quad (15)$$

and that for $\mu_s = 0.0125''$ it implies 80 effective flaws to the inch. The choice of the standard deviations is a matter of adjusting to the actual data scatter [51].

As for the laminates of $n = 1$, the thickness of the 90° -layer is only $0.0104''$, or $a_o < 0.0052''$. For this case, the choice of μ_a and σ_a are as follows:

$$\mu_a = 0.0021'', \sigma_a = 0.0075'' \quad (16)$$

so that

$$a_o = \mu_a + 3\sigma_a = 0.0044'' \quad (17)$$

The choice of the spacing parameters remains the same for $n = 1$.

The Monte-Carlo simulation procedures start with the generation of a set of N ($= 80$) flaws whose random sizes and spacings are represented by the respective density functions (9) and (10). This is done by generating first a set of N random values in the interval $(0,1)$. Then, by equating the cumulative function of $f(a)$ to each of the random values, a random set $\{a_i\}$, $i = 1, N$ is computed. Among the values in $\{a_i\}$, the probability of the largest to be equal or greater than a_0 as defined in (15) or (17) is about 99%.

Similarly, a random set $\{S_i\}$, $i = 1, (N - 1)$, is also generated by the random number scheme. S_i is then assigned to be the spacing between the i th and the $(i + 1)$ th flaws.

Thus, a computer research follows, which determines the flaw most likely to become a transverse crack. The first to occur, clearly, is the worst flaw in the $\{a_i\}$ set, and the corresponding applied load for the onset of the first crack is then determined using Equation (11).

After the first crack is formed, another flaw in the $\{a_i\}$ set will become a crack at a slightly higher load. But this flaw is located at a random distance from the first crack. And the presence of the physical (real) crack has a stress reducing effect on the rest of the flaws. Thus, if the second flaw to become a crack is located outside the shear-lag zone, it will not feel the presence of the first crack; and hence, its available energy release rate at the instant of cracking is given by $G_0(\sigma, a)$, the same as in Equation (8).

On the other hand, if the second flaw is located inside the shear-lag zone, then the available energy release rate is reduced by a factor de-

pending on its distance from the first crack.

Generally, for the flow to become the kth crack, one must search to the left and to the right for the nearest cracks. If so, the energy release rate at the instance of the kth crack is given by

$$G_k(\sigma, a) = R(S_l) G_o(\sigma, a) R(S_r) \quad (18)$$

where S_l is the distance to the left crack, S_r the distance to the right crack.

In Equation (18), $R(S)$ is the energy rate retention factor which is generated by the finite element routine for a flaw of $2a$ ($<2a_o$) and is placed at varying distance S from a transverse crack, see Figure 9.

For the laminate family $[0_2/90_n]_s$, a single $R(S)$ curve can be generated if expressed in terms of S/nt , t being the thickness of one 90° -ply, see Figure 9. Note that 100% energy rate retention is expected beyond $S = 9nt$; the latter is actually the size of the shear-lag zone [19].

The applied load, corresponding to the kth crack is determined from

$$G_k(\sigma, a) = G_c \quad (19)$$

The search essentially simulates the cracking process as it would occur naturally. Each random simulation represents an actual test case; and repeated simulations present actual tests on replicas.

Figures 10, 11, and 12 show the simulated crack-density versus load plots for respectively, $[0_2/90]_s$, $[0_2/90_2]$ and $[0_2/90_3]$ laminates. In the simulations, the quantities appearing in Equation (11) are assigned as follows:

$$\Delta T = 225^{\circ}\text{F}, t = 0.0052", G_c = 1.3 \text{ lb/in} \quad (20)$$

The shaded band in each of these plots is the corresponding experimental data band from 4 test specimens. These test data were reported earlier in Reference [52]; and the details for the simulation computer routine are reported in Reference [51].

MECHANICS OF FREE EDGE DELAMINATION

The Classical Free-Edge Problem

The free edge delamination problem has attracted increased research interests ever since the advent of composite laminates. The phenomena are frequently observed as the most damaging sub-laminate failure mode. Generally, it is a plane crack which forms along the laminate free edge and propagates inward along an interface of two adjacent layers.

Figure 13 shows an x-ray plane view of a $[\underline{+45/0/90}]_s$ graphite-epoxy laminate under uniaxial tension (left). Delamination is seen to occur along both edges of the laminate, with essentially uniform growth toward the center. An edge view of this crack is shown on the right, which indicated that the crack is basically contained inside the 90° -layer, not necessarily in any one given layer interface. Moreover, the cracked plane is quite zig-zagged along the length of the free edge.

Similar photographs, taken for a $[\underline{+25/90}_{1/2}]_s$ laminate after failure, are shown in Figure 14. Here, the edge crack is seen to have formed inside the 90° -layer, but branched to the $25/90$ interface as it propagated. The branch-out is due to the skewed cracks which occur in the 90° -layer ahead of the edge delamination front.

Note that both laminates have a 90° -layer; and they could suffer transverse cracking under the tensile load. But, because the thickness of the 90° -layer is thin, a high load is required for transverse cracking according to the energy theory presented earlier. Instead, in this case, edge delamination is induced as the first event of sub-laminate failure.

Analytical studies of the free edge delamination problem have originated from the much celebrated work of Pipes and Pagano [53], who formulated and computed the boundary-layer interlaminar stress solutions for a long symmetric laminate under tension. The formulation is based on the macroscopic ply-elasticity theory, which regards the material layers as individually homogeneous media; material and geometrical discontinuities exist only across the layer interfaces.

Generally, the free edge stress field is three-dimensional, and is singular at the intersect of the free-edge with the layer interface [36]. Hence, interface delamination is caused by the highly concentrated edge stresses, especially the interlaminar normal stress σ_z .

In a series of tensile strength tests, Bjeletich, et. al. [54] examined the failure modes of six families of quasi-isotropic laminates by alternating the stacking sequence of the 0° , 90° and $\pm 45^\circ$ layers. Edge stress analysis indicated a compressive σ_z along the free edge of the $[0/90/\pm 45]_s$ laminate, while a tensile σ_z for the $[\pm 45/0/90]_s$ laminate. The latter developed prematured delamination; and the growth of it had led to a much lowered tensile strength. Clearly, knowledge of the free-edge stresses can provide an explanation why delamination occur; but a quantitative prediction for its occurrence requires a more precisely defined criterion.

In a study on delamination for similar graphite-epoxy laminates, Rodini, et. al. [55] determined experimentally the critical tensile loads at the onset of free edge delamination in a $[\underline{+45}_n/0_n/90_n]_s$, $n = 1, 2, 3$ family. They found that the critical laminate tensile stress $\bar{\sigma}_x$ varied greatly with the value of n . Specifically, the critical $\bar{\sigma}_x$ decreases at the rate of about \sqrt{n} , even though an edge stress analysis yields identical $\bar{\sigma}_z$ for the same $\bar{\sigma}_x$ for all values of n .

Such a 90° -layer thickness dependent behavior is similar to that found in the transverse cracking problems, suggesting the observed phenomenon is again fracture in nature.

The Energy Criterion

In the work of Wang and Crossman [18], it is assumed that material flaws exist randomly on any one of the interfaces between the material layers. Those flaws which are located within the free-edge stress zone form an "effective" flaw having a size a_0 at the instance of onset of delamination, see insert in Figure 15. Following the finite element crack-closure procedure by allowing virtual extension of a_0 along the layer interface, an energy release rate curve is generated, such as shown in Figure 15.

It is seen that the energy release rate G increases sharply with a , but reaches an asymptote at $a = a_m$. Generally, the value of a_m is about one-half the layer-thickness which contains the delamination [18]. Thus, the layer thickness affect the value of a_m , and also the value of G .

Expressing the computed energy release rate, Equation (6),

$$G(e_0, a) = C_E(a) \cdot t \cdot e_0^2 \quad (21)$$

and applying the Griffith criterion (3) for the onset of delamination, one obtains the critical far-field strain.

$$(e_o)_{cr} = [G_c / C_E(a) \cdot t]^{1/2}, \quad a = a_o \quad (22)$$

Note that in (22), the thermal residual effect is not included. In most laminates, thermal effect on delamination is minimal [56].

The problem comes down to two important questions; namely, what value is a_o , and in which interface is it located?

To answer the first question, recall the earlier discussions about a_o in unbounded 90° laminates. As inferred from the Griffith's criterion, a_o is in the order of 0.01", or 2 times the ply thickness for commercial graphite-epoxy systems. It is believed that a_o for delamination is at least of this magnitude if not larger, because of possible additional cutting flaws along the free edge. In any event, if a_m in Figure 15 is less than 3 times of the ply thickness, one simply uses $a = a_m$ and predicts from Equation (22) the minimum possible load for the onset of delamination. Thus

$$(e_o)_{cr} = [G_c / C_E(a_m) \cdot t]^{1/2} \quad (23)$$

The answer to the second question, however, is complicated, if not inconclusive. Consider as an example a $[90_2/0_2/+45_2]_s$ under uniform compression. Interlaminar tensile σ_z is developed in this laminate and edge delamination is induced before global buckling, see Figure 16. A 3-dimensional through-thickness display of σ_z is shown in Figure 17. It is seen that the largest σ_z is located on the 45/-45 interface (in fact, this σ_z

is singular at the free edge). On the other hand, σ_z along the mid-plane ($z = 0$) is finite at the free edge. In addition, there is also a singular interlaminar shear stress τ_{xz} along the 45/-45 interface as the most probable analysis suggests the 0/45 interface as delamination site.

However, according to the energy release rate argument as well as the "effective" flaw hypothesis, one must reply upon the calculated energy release rate curve such as shown in Figure 15, in order to define which one of the interfaces is likely to delaminate.

The finite element crack-closure results of the $G(a)$ curves for this example problem is shown in Figure 17. Indeed, the interface that yields the highest energy release rate is the mid-plane ($z = 0$), not the 45/-45 interface. Besides, a delamination in the mid-plane is in mode-I, while it is mixed-mode (I, III) in the 45/-45 interface. As has been discussed earlier, mixed-mode G_c is usually higher than G_{Ic} . Thus, the mid-plane is the predicted delamination site, not the 0/45 interface.

This conclusion is confirmed by experiments conducted by Wang and Slowiana [57], who also investigated compression-induced delamination in $[0_2/90_2/\pm 45_2]_s$ and $[0/90/0/90/\pm 45/\pm 45]_s$ laminates. In all cases, mid-plane and mode-I delamination was predicted and observed. Using the energy criterion of Equation (23), and setting $G_c = 1.3$ lb/in, their predicted minimum onset loads ($\bar{\sigma}_x$) compared well with the experimental findings (average of 3 specimens):

| <u>Laminates</u> | <u>Predicted onset of $\bar{\sigma}_x$</u> | <u>Experimental Finding</u> |
|-------------------------------|---|-----------------------------|
| $[90_2/0_2/\pm 45_2]_s$ | 43.9 ksi | 45.7 ksi |
| $[0_2/90_2/\pm 45_2]_s$ | 50.9 | 52.0 |
| $[0/90/0/90/\pm 45/\pm 45]_s$ | 59.1 | 62.0 |

Edge Delamination and Transverse Cracking: Their Interactions

In the previous examples, edge delamination is the first and only sub-laminate failure mode before laminate buckling. The onset load for delamination is synonymous to the final laminate failure load. In most other cases, edge delamination and transverse cracking are often two competing failure modes, which interact each other through a complicated mechanisms.

Examine again the photomicrographs shown in Figures 13 and 14, where a $[+45/0/90]_s$ and a $[+25/90_{1/2}]_s$ laminates were loaded by axial tension. The thickness of the 90° -layer in both laminates is so small that transverse cracking is possible only at a high load. Instead, an edge delamination is induced as the first sub-laminate failure mode. Nonetheless, the stress field in the 90° -layer, which contains the delamination, appears to be extremely complex. The skewed cracks shown in Figure 14 are indicative of the complex stress field ahead of the delamination front. But, just how profoundly these secondary cracking events influence the delamination growth is far from known.

On the other hand, Figure 18a shows an x-ray plane view of a $[+25/90_2]_s$ laminate after delamination. Actually, this laminate suffered first transverse cracks in the 90° -layer; subsequent edge delamination in the $25/90$ interface developed at a higher load. It is seen from the picture that delamination actually caused many more transverse cracks because of stress concentration along the curved delamination front. In the area where delamination had not occurred, only a few transverse cracks are visible. This phenomenon has repeatedly been observed in experiments [21]; but no serious account has been attempted to analytically modelling it.

Law [56] assumed that when transverse cracks occur in the 90° -layer, the tensile modulus E_T and the Poisson ratio ν_{TL} of the 90° -layer both reduce to nearly zero. With reduced moduli in the 90° -layer, the overall laminate becomes energetically delamination prone in the 25/90 interface, resulting in a mixed-mode cracking (I, II). Law was able to predict the onset loads for this and other similar cases in an approximate manner.

Figure 18b shows an x-ray plane view for a $[\pm 25/90_4]_s$ laminate soon after transverse cracking took place. In this case, scattered transverse cracks appeared first, which immediately caused delamination on both 25/90 interfaces in the area where they occurred. The delamination is, in fact, a combined effect stemming from the transverse crack-tip and free edge stress concentrations. Figure 19 illustrates this combined effect in an isometric view. The interface shear stress τ_{xz} , which is developed at the transverse crack root, tends to delaminate the 25/90 interface in the x-direction; and the interlaminar normal stress, σ_z , which is a free edge effect, tends to open up the same interface in the y-direction. The combined action gives rise to a mixed-mode, delta-shaped delamination. Evidence of this type of delamination can be found by examining Figure 18b.

Law [56] approximated the combined effect by first computing G_x for the x-direction delamination by a 2-dimensional analysis, and then by computing G_y for the y-direction as in the case of free edge delamination. Since both G_x and G_y are considered crack-driving forces, their vector sum is used to predict the onset of the delta-shaped delamination. Obviously, such an approximate approach is only tentative; the problem remains to be treated more rigorously by a 3-dimensional analysis which can simulate a contoured plane delamination. But, as it will be shown in the next section, Law's approach was at least qualitatively correct.

It is now apparent that sub-laminate crackings, especially delamination, are physically complicated even under simple tension. The energy model presented earlier may be applied only in cases where a single failure mode is present. Interactions amongst multiple failure modes are yet to be investigated more extensively.

An Experimental Case Study

An experimental case study on transverse cracking, free edge delamination and their mutual interaction was conducted by Crossman and Wang [21]. They chose a family of graphite-epoxy laminates (T300/934) in the form of $[\underline{+25/90}]_n$. By varying the single parameter $n = 1/2, 1, 2, 3, 4, 6$ and 8 , they were able to control the occurrence of the various competing failure modes in the laminates when loaded in tension. Both x-radiography and microphotography were used to monitor the sub-laminate cracking development as a function of the applied load. For clarity, a graphical summary of their experimental findings is shown in Figure 20. For $n = 1/2$ and 1 , the laminates are classified as having a "thin" 90° -layer. Transverse cracking is suppressed due to the lack of sufficient strain energy stored in the 90° -layer. Hence, free edge delamination occurs as the first sub-laminate failure mode. For $n = 1/2$, a stable mode-I delamination is produced during the loading until final failure. For $n = 1$, however, transverse cracks are induced in the area of delamination. Because of these cracks, the delamination plane is often branched to the $25/90$ interface. This latter appearance is indicative of an interaction taking place between the two failure modes.

When $n = 2$ and 3 , the laminates are denoted as having "thick" 90° -layer. In both, transverse cracks occur first long before delamination. It may be thought that the onset of transverse cracking is an independent

event, while delamination is caused, at least partially, by the presence of the multiple transverse cracks. Indeed, the delamination plane in the case of $n = 2$ resembles that for $n = 1$; and the delamination plane in the $n = 3$ laminate is entirely in the 25/90 interface. Also, for $n = 3$, the growth of delamination becomes more rapid.

The laminates with "very thick" 90°-layer are those for $n = 4, 6,$ and 8. In all cases transverse cracks occur first followed immediately by delta-shaped delaminations emanating from the transverse crack roots. These soon coalesce to form large scale 25/90 delamination, resulting in prematured laminate failure.

Figure 21a summarizes the various onset loads for each types of the laminates (signified by the value of n). Since the laminate stress-strain response for all cases is essentially linear until final failure, it is convenient to use the laminate tensile strain, $\bar{\epsilon}_x$ as a measure of the applied load. Note that except for $n = 1/2$ and 1, transverse cracking is the first sub-laminate failure event. Generally, growth of multiple cracks is fully developed, followed by interlayer delamination. However, as $n > 3$, the load-gap between the transverse cracking and delamination events grows closer. In fact for $n = 8$, these two events are so closely linked as to cause immediately final failure.

Note also that except for $n = 1/2, 1$ and 2, onset of delamination and final failure are separated only by less than 5% of loading.

By means of the energy model presented earlier, Law [56] conducted a computer simulation of the transverse cracking and delamination processes in the $[\underline{+25/90}_n]_s$ family. The numerical results are shown in Figure 21b, which is superscribed on the experimental results shown in Figure 21a.

Law has conducted four different types of crack simulations: (a) onset of transverse cracking in the 90° -layers for all values of n ; (b) mid-plane ($z = 0$), mode-I delamination for $n = 1/2, 1, 2,$ and 3 ; (c) $25/90$ interface delamination for $n = 2, 3,$ and 4 (the 90° -layer is saturated with transverse cracks; and is represented by reduced moduli); and (d) transverse crack root/free edge combined delamination of the $25/90$ interface for $n = 3, 4, 6$ and 8 (as illustrated in Figure 19).

It is seen from Figure 21b that the predicted onset loads for transverse cracking agree well with the experiment, while the predicted delamination loads (represented by 3 curves) form an envelope to which the experimental points fall below. Although the predicted delamination loads for $n = 6$ and 8 are off considerably from the experimental points, the energy analysis seems to capture the physical mechanisms of these various failure modes; the analysis gives correctly the trend of the failure loads.

Final Failure Mechanisms

In the case study discussed above, the sub-laminate failure sequence is seen to lead to the final rupture of the laminate. It is generally thought that final failure is determined practically by the strength of the load-carrying plies; i.e. in the case of the $[\pm 25/90_n]_s$ family, the ± 25 -plies should carry essentially all the load. But, what determines the strength of the ± 25 -plies? And, is it adversely influenced by the sub-laminate cracking events that preceded the final laminate rupture? These questions relate to the final failure modes and their associated fracture mechanisms.

Crossman [58] conducted recently an extensive experimental investigation into the failure sequence of several families of laminates under uni-

axial tension. Some of his results may help to answer the above questions.

Consider first the effect of thickness of the load-carrying plies by examining the results in Table A.

It is noted that the final failure mode of $[\underline{+25}/\underline{+25}]_s$ is due simply to fiber breaking across the laminate, while the final failure mode of $[25_2/\underline{-25}_2]_s$ involves a major transverse crack in the center core (-25_4° -layer) followed by multiple fiber-splitting in the 25_2 -layer. In particular, there is no fiber breakage involved in the latter case, see Figure 22.

An energy analysis of the respective failure modes indicated that the transverse cracking mode in the $[\underline{+25}/\underline{+25}]_s$ is suppressed by the actual thickness of the 25° -layer; there is not enough strain energy to cause this failure mode at a lower load level. Hence, it forces a fiber breakage instead. However, by doubling the layer thickness, in the case of $[25_2/\underline{-25}_2]_s$, the transverse cracking mode emerges at a much lower load. The difference in the failure modes results in the difference in the applied ultimate loads.

Clearly, the strength of the so-called "load-carrying" plies in a laminate depends also on the particular fracture modes that cause failure. In the examples above, the ply-thickness factor is seen again to play a profound role in the final failure mechanisms.

When the respective load-carrying plies are laminated with a 90° -layer, such as in $[\underline{+25}/\underline{+25}/90_2]_s$ and $[25_2/\underline{-25}_2/90_2]_s$, transverse cracks in the 90° -layer and edge delamination are found to proceed any failure in the 25° -plies. From the results displayed in Table A, it is seen that the sub-laminate cracking events neither changed the failure mode of the $\underline{+25^\circ}$ -plies, nor decreased the final ultimate loading. Furthermore, the presence of the 90° -layer in $[25_2/\underline{-25}_2/90_2]_s$ actually increased the lami-

nate load-carrying capacity. The reason is that $[25_2/-25_2]_s$ has four (4) 25°-plies in the core, while $[25_2/-25_2/90_2]_s$ has only two (2) 25°-plies scattered by the presence of the 90°-layer in the core.

However, adverse effects of sub-laminate cracking on laminate final failure modes are seen from the test results displayed in Table B. Here, the failure modes in $[+θ/90_2]_s$ and $[+θ/90_8]_s$ are compared. Note that the 90°-layer thickness in the latter is exaggerated in order to separate widely the respective sub-laminate crack modes.

In the cases of $[0_2/90_8]_s$ and $[+25/90_8]_s$, the final failure mode in the load-carrying plies involves multiple fiber-splitting, which occur along the root of a 90°-layer transverse crack; see Figure 22. On the other hand, there is no fiber-splitting in the $[0_2/90_2]_s$ or the $[+25/90_2]_s$ laminates.

A three dimensional stress analysis will show that there is a stress concentration at the 90°-layer transverse crack root; both the applied tension and thermal cooling contribute to the stress concentration. In particular, the size of the stress concentration zone is proportional to the 90°-layer thickness; which explains why the considerable difference in the final loads between $[0_2/90_2]_s$ and $[0_2/90_8]_s$; and between $[+25/90_2]_s$ and $[+25/90_8]_s$, see Table B.

Fiber-splitting seems to be the striggering failure mode in the $[0_2/90_8]_s$ and $[+25/90_8]_s$ laminates. The splitting mechanisms is due to the existance of the tensile stress normal to the fibers, which is magnified in amplitude by the 90°-layer transverse crack root.

Similar stress condition also exists in the $[+30/90_8]_s$ laminates. But in this case, the tensile stress (normal to $±30°$ -fibers) is not large enough

to cause fiber splitting; see also Table B. As a result, the final failure modes for $[\underline{+30/90}_2]_s$ and $[\underline{+30/90}_8]_s$ all involve fiber breaking; and their final failure load are essentially the same. Thus, a mere increase in the angle from 25° to 30° changes the failure mode.

Clearly, the final failure modes in the "load-carrying" plies can be influenced by nature from the sub-laminate crackings. Moreover, there are probably a host of other possible modes that are competing for dominance. The specific failure occurrence in a given laminate is generally determined by the lamination geometry as well as the intrinsic material properties. And, of course, there are always the statistical uncertainties in the "intrinsic" material properties.

CONCLUSIONS

This paper has attempted to give an overview of a fracture mechanics approach to some of the frequently observed sub-laminate cracks in epoxy-based composite laminates. The laminates discussed in the paper served mainly to illustrate how a certain simple failure sequence is developed and how the predictive model is constructed. They are certainly not ones which may be used in practical design applications. The main objective is to enable to see through the various fracture mechanisms and try to understand them; at times, one even exaggerates the geometric parameter to a radical extent.

Indeed, the field of fracture in composites seems infinitely complex. Yet, numerous past and present investigators have toiled the field with many successes. And, new discoveries are being continuously made to further its advancement. The results reported in this paper represent but one effort to fill the dimensional span from micromechanics to structural mechanics in composite failure analysis.

Acknowledgments. Many results reported in this paper were obtained in collaboration with Drs. F. W. Crossman, G. E. Law, H. Miller and N. N. Kishore; and with Mr. C. Lei and Ms. M. Slomiana, graduate students at Drexel University. Financial supports have been provided by the U. S. Air Force Office of Scientific Research, Wright Aeronautical Laboratory and the Naval Air Development Center.

TABLE A

| <u>Laminate</u> | <u>Sequence of Failure Modes</u> | <u>Total load in lbs.</u> |
|--|--|--|
| $[\underline{+25}/\underline{+25}]_s$ | no transverse cracking no edge delamination cross-section fiber break | <u>3103(2895-3245)</u> |
| $[25_2/\underline{-25}_2]_s$ | single transverse crack in -25-layer, followed by multiple transverse cracks in the +25-layer | occur at 98% P_u |
| | final failure involved no fiber break | <u>2272(2001-2480)</u> |
| $[\underline{+25}/\underline{+25}/90_2]_s$ | transverse cracks in 90-layer stable edge delamination | occur at 80% P_u occur at 90% P_u |
| | cross-section fiber break in the 25-layers | <u>3040(3001-3250)</u> |
| $[25_2/\underline{-25}_2/90_2]_s$ | transverse cracks in 90-layer rapid edge delamination | occur at 90% P_u occur at 98% P_u |
| | fiber-split in 25-layer | <u>2648(2500-2830)</u> |

TABLE B

| <u>Laminate</u> | <u>Sequence of failure modes</u> | <u>Total load in lbs.</u> |
|----------------------------|---|--|
| $[\underline{+25/90}_2]_s$ | transverse cracks in 90-layer stable edge delamination cross-section fiber break in 25-layers | occur at 85% P_u occur at 95% P_u <u>1802(1747-1893)</u> |
| $[\underline{+25/90}_8]_s$ | scattered transverse cracks local delamination from T.C. tip; combined with edge delam. fiber split in 25-layer few fiber break in 25-layer | occur at 95% P_u <u>1606(1500-1660)</u> |
| $[0_2/90_2]_s$ | transverse cracks in 90-layer no edge delamination cross-section fiber break of 0-layer | occur at 80% P_u <u>5163(4600-5730)</u> |
| $[0_2/90_8]_s$ | scattered transverse cracks local delamination from T.C. tip; local fiber-split in 0-layer above transverse crack coalescence of fiber-splits in 0-layer final 0-layer failure | occur at 75% P_u occur at 85% P_u <u>4220(4120-4320)</u> |
| $[\underline{+30/90}_2]_s$ | transverse crack in 90°-layer stable edge delamination cross-section fiber break in 30-layer | <u>1650(1625-1670)</u> |
| $[\underline{+30/90}_8]_s$ | transverse crack in 90°-layer local edge delamination from T.C. tip; fiber break in 30-layer | <u>1622(1620-1625)</u> |

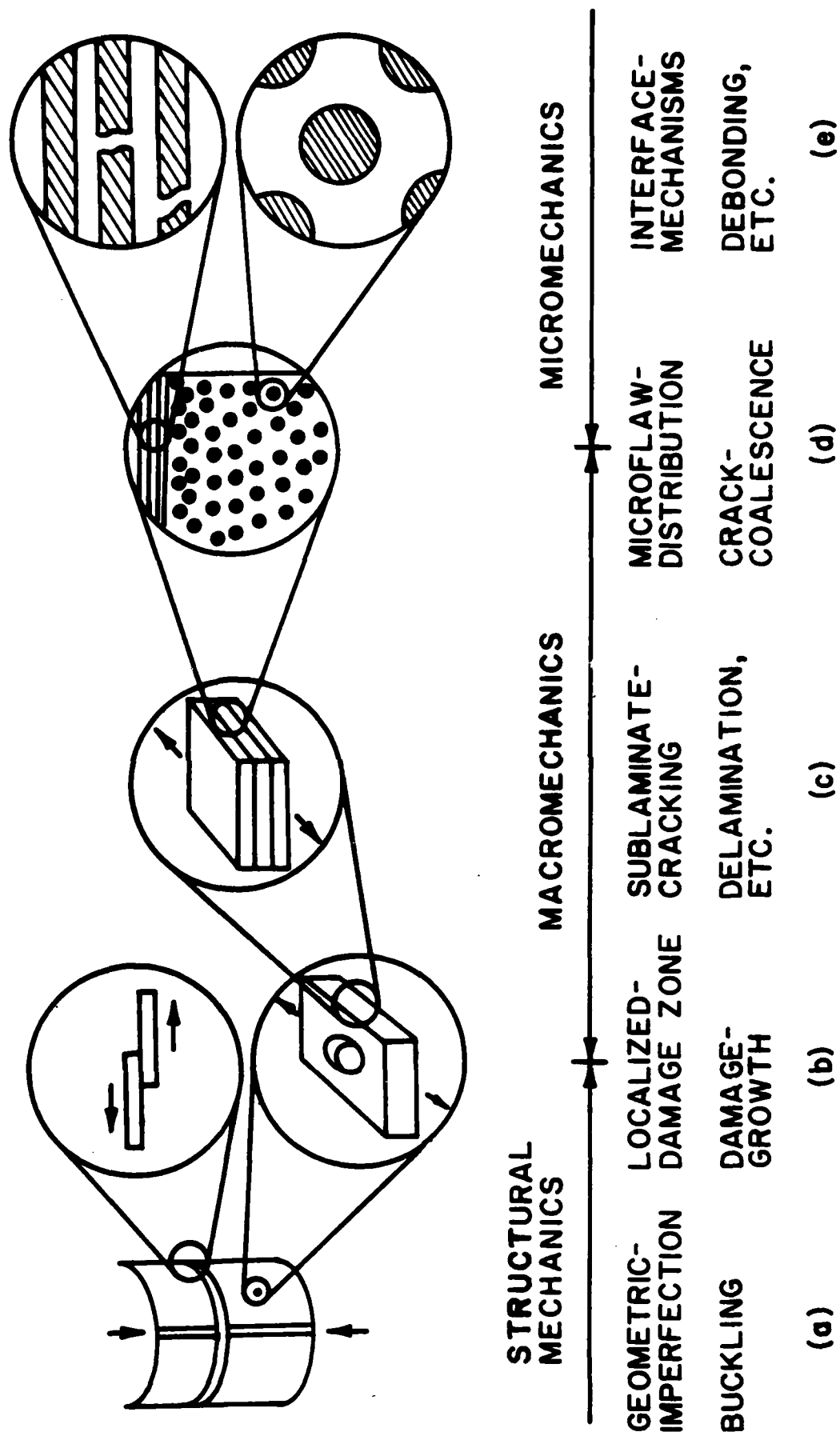


Fig. 1 Dimensional Regimes of Failure Analysis in Composite Materials

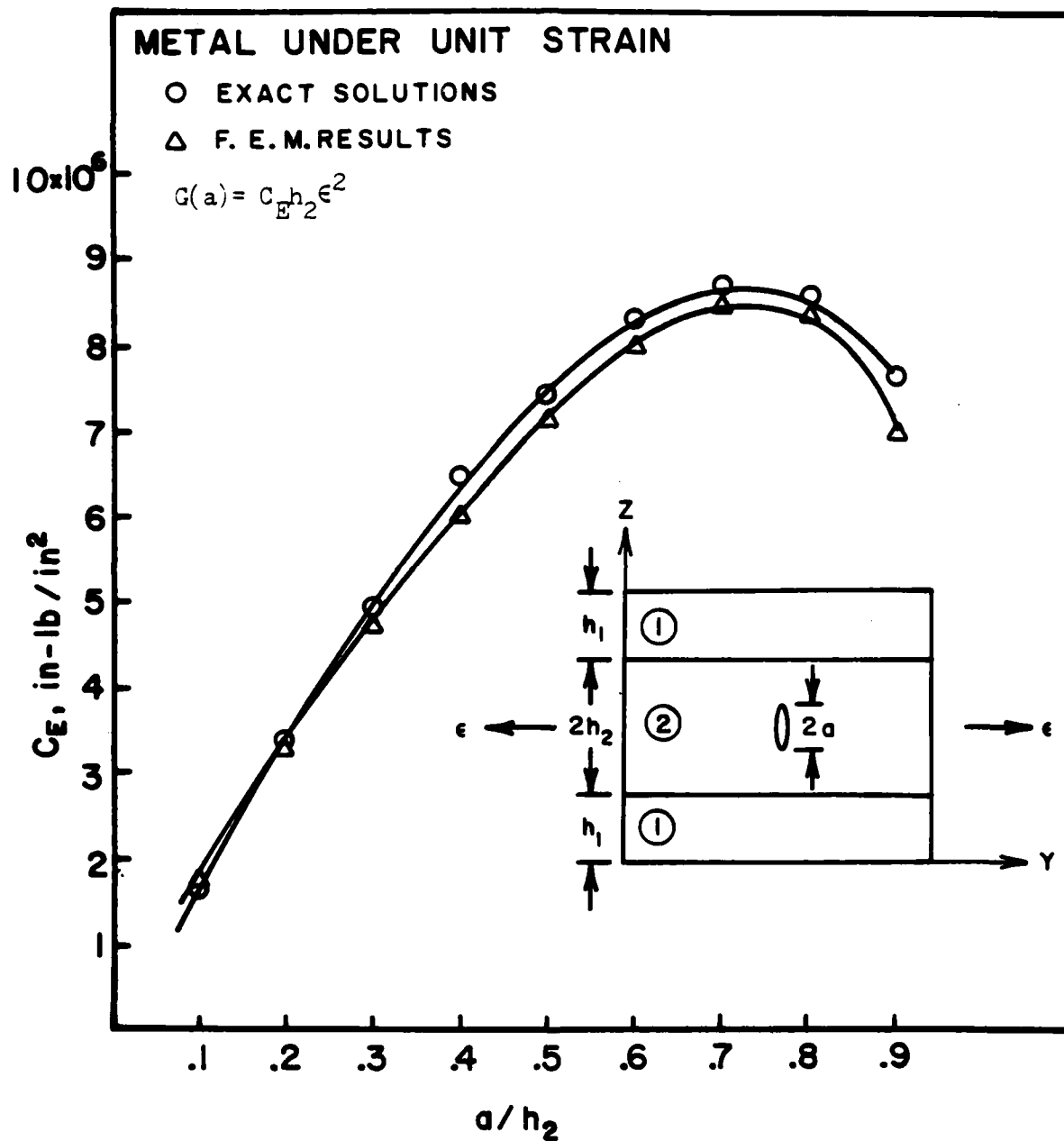


Fig. 2 Comparison of the Exact and the Finite Element Solutions for $G(a)$; $E_1/E_2 = 5$; $h_1 = h_2$; $\nu_1 = \nu_2 = 1/3$.

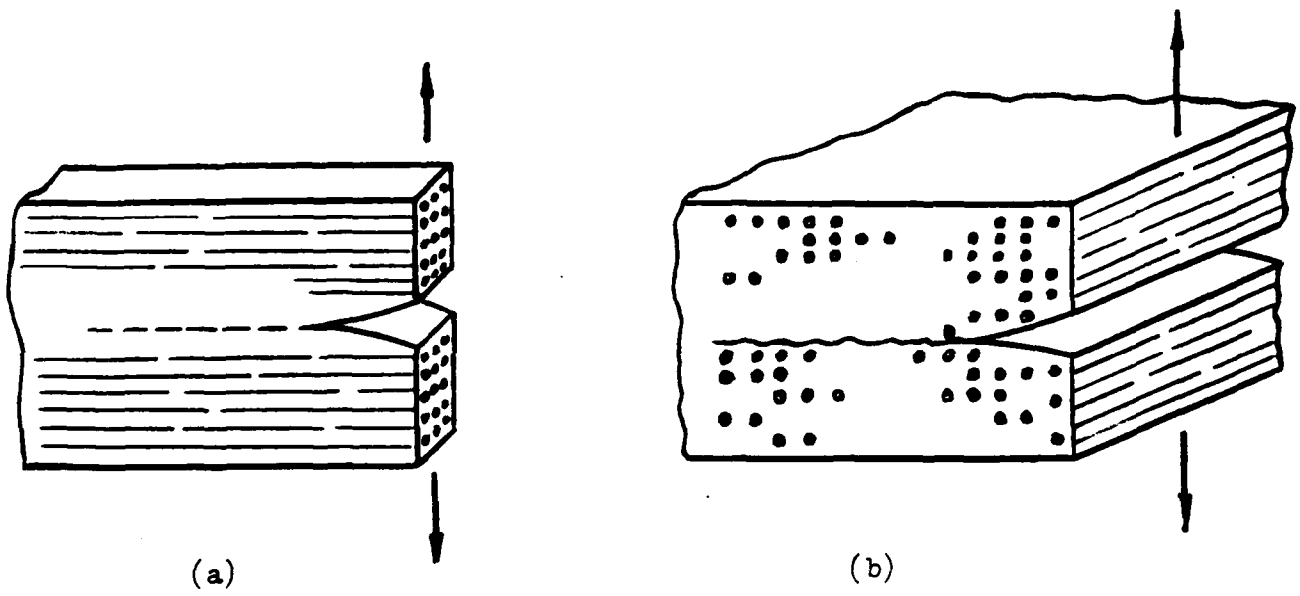


Fig. 3(a) $0^{\circ}/0^{\circ}$ Mode-I Delamination; (b) $90^{\circ}/90^{\circ}$ Delamination.

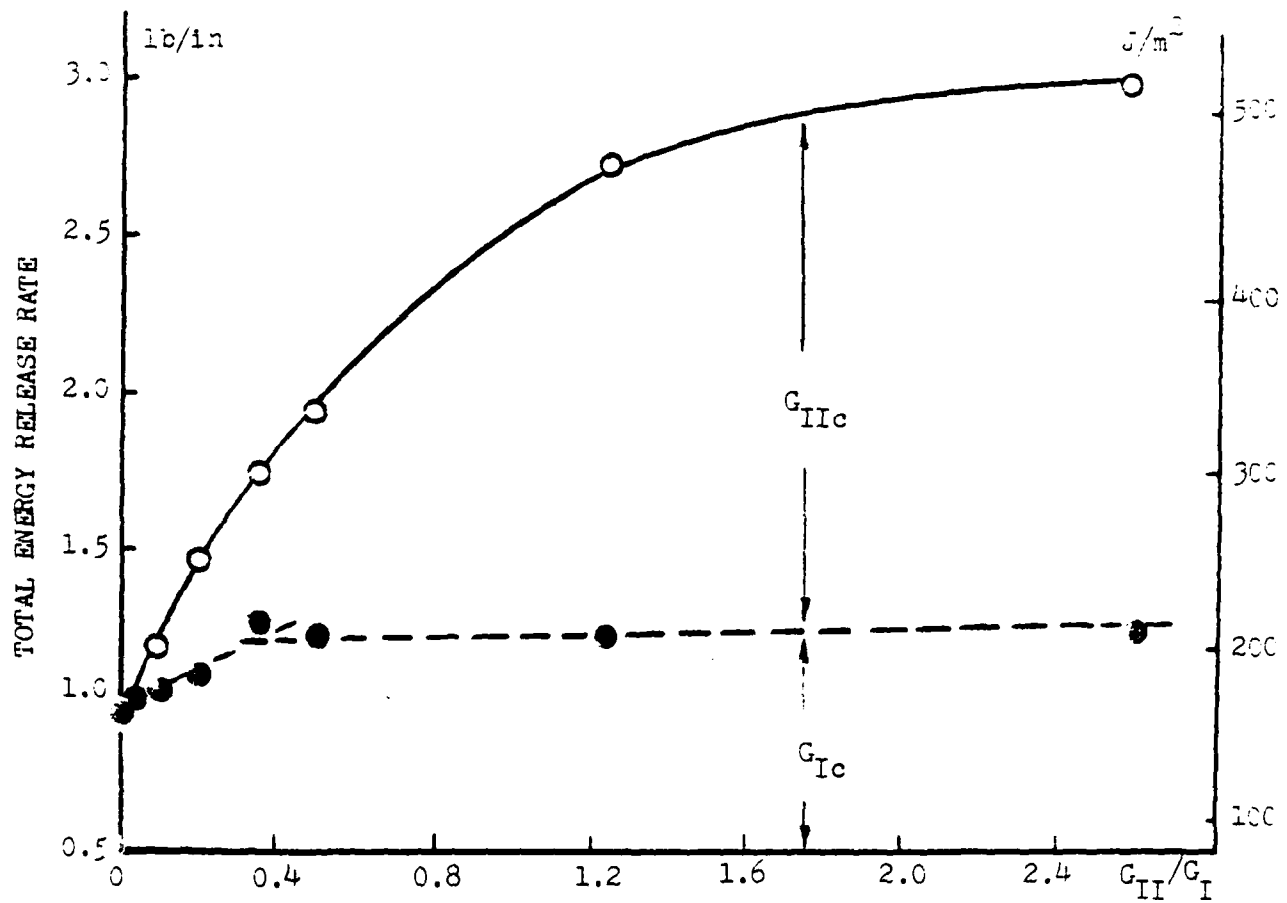


Fig. 4 Mixed-Mode $G_c (= G_{Ic} + G_{IIc})$ vs. G_{II}/G_I Ratio.

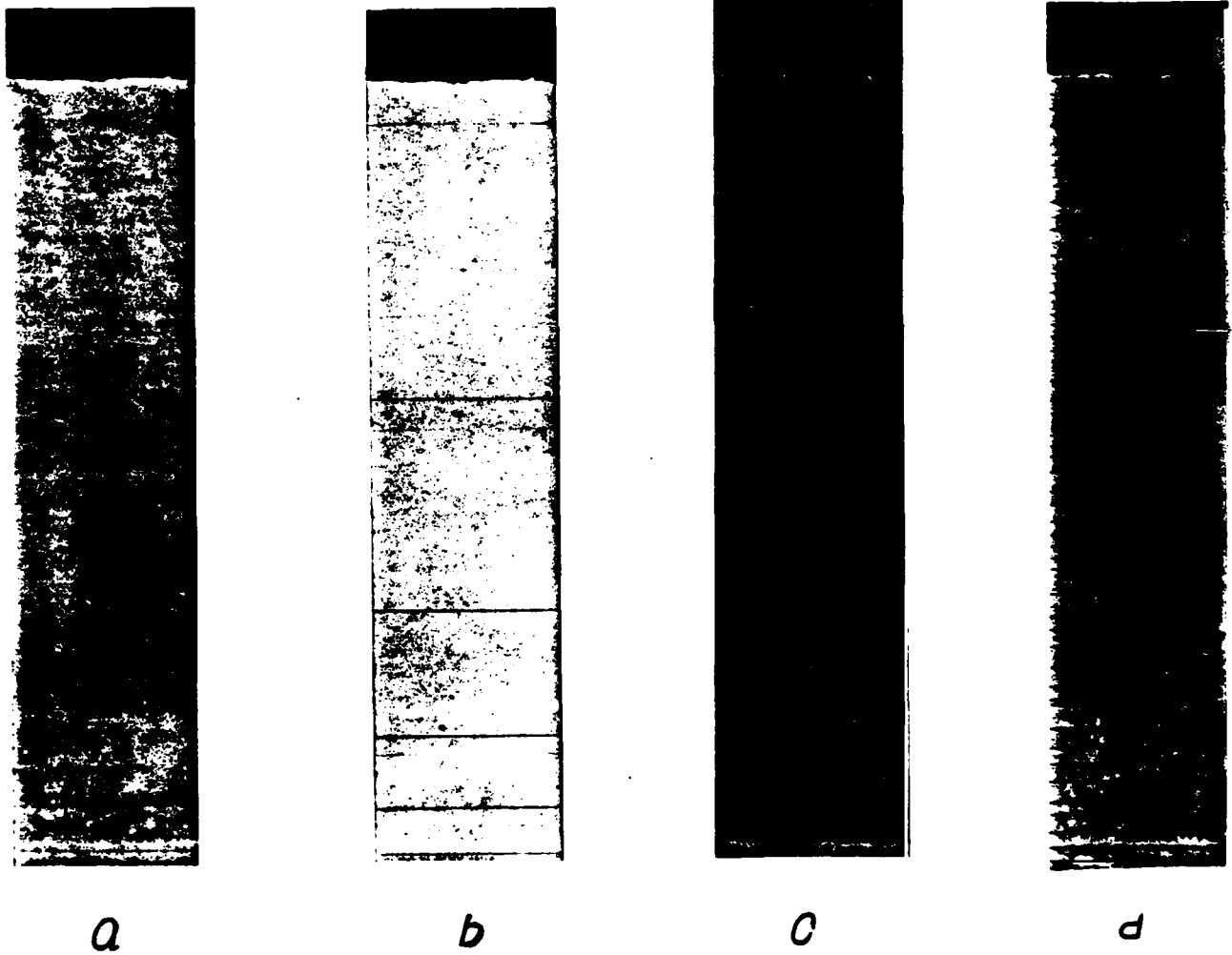


Fig. 5 X-Radiographs of Transverse Cracks Formation Under Increasing Loading. T300/934 [0/90]_s Laminate.

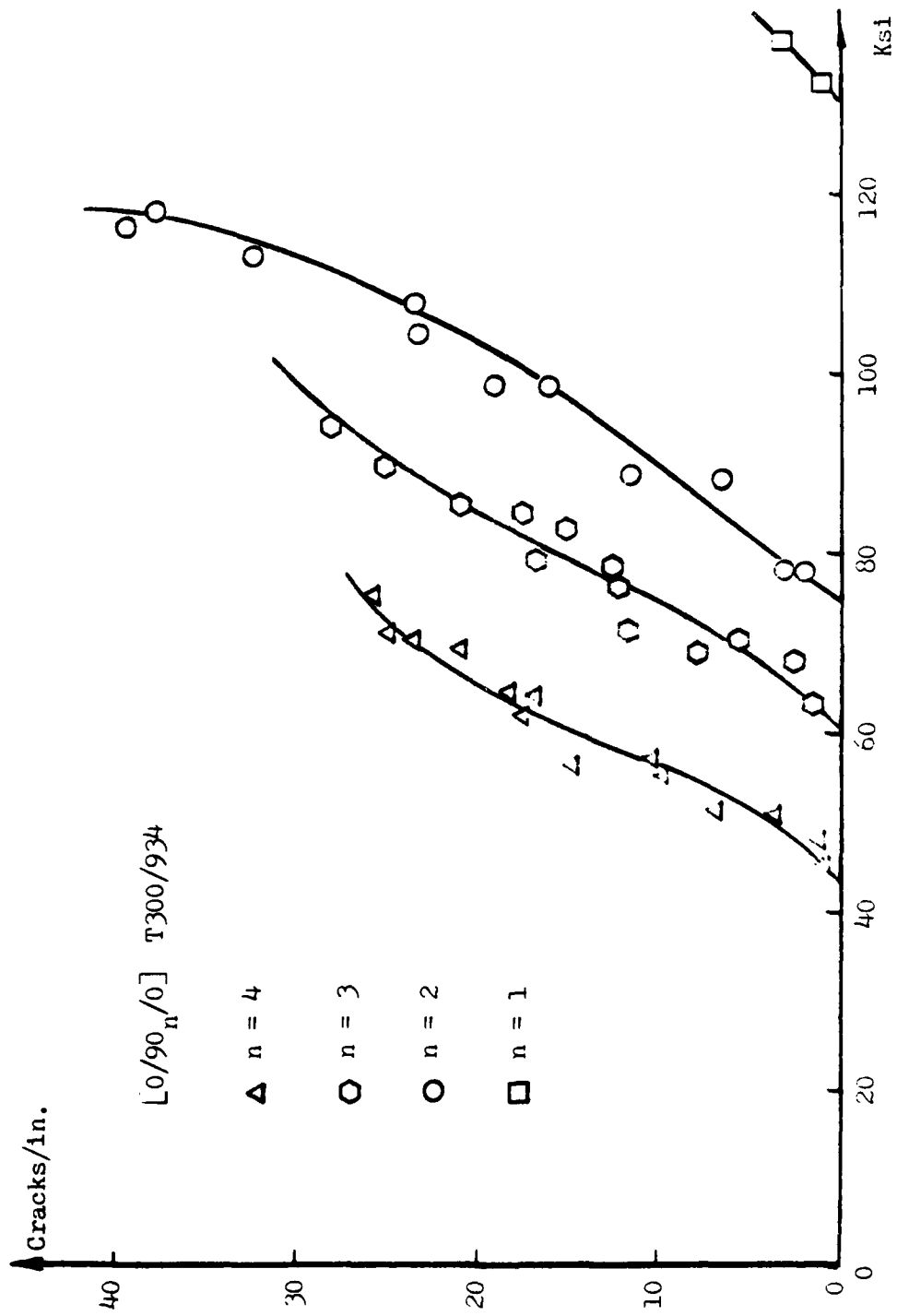


Fig. 6 Transverse Crack Density vs. Applied Tensile Stress.

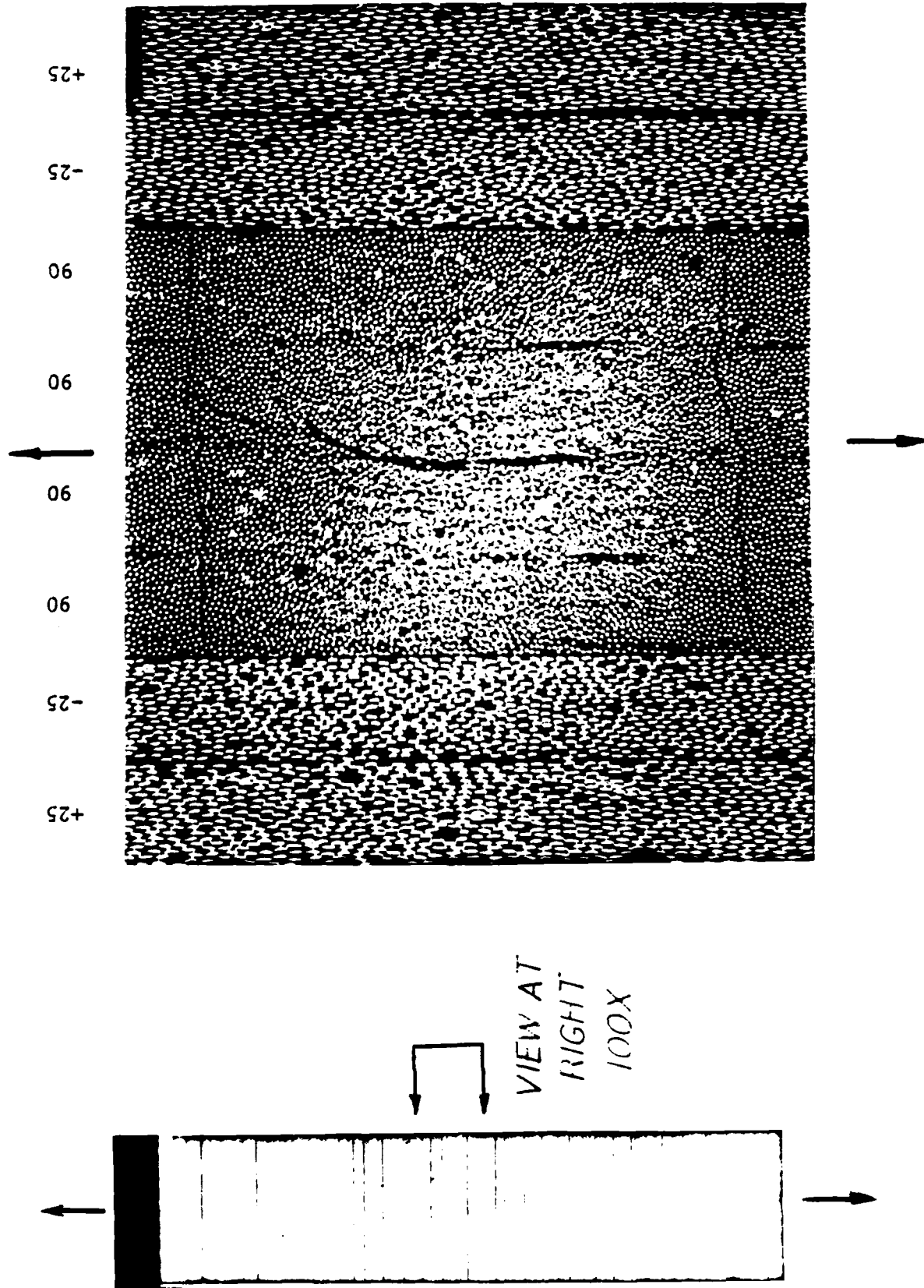


Fig. 7 Micrograph(right) Showing Two Transverse Cracks In A $[+25/90_2]$ Laminate.

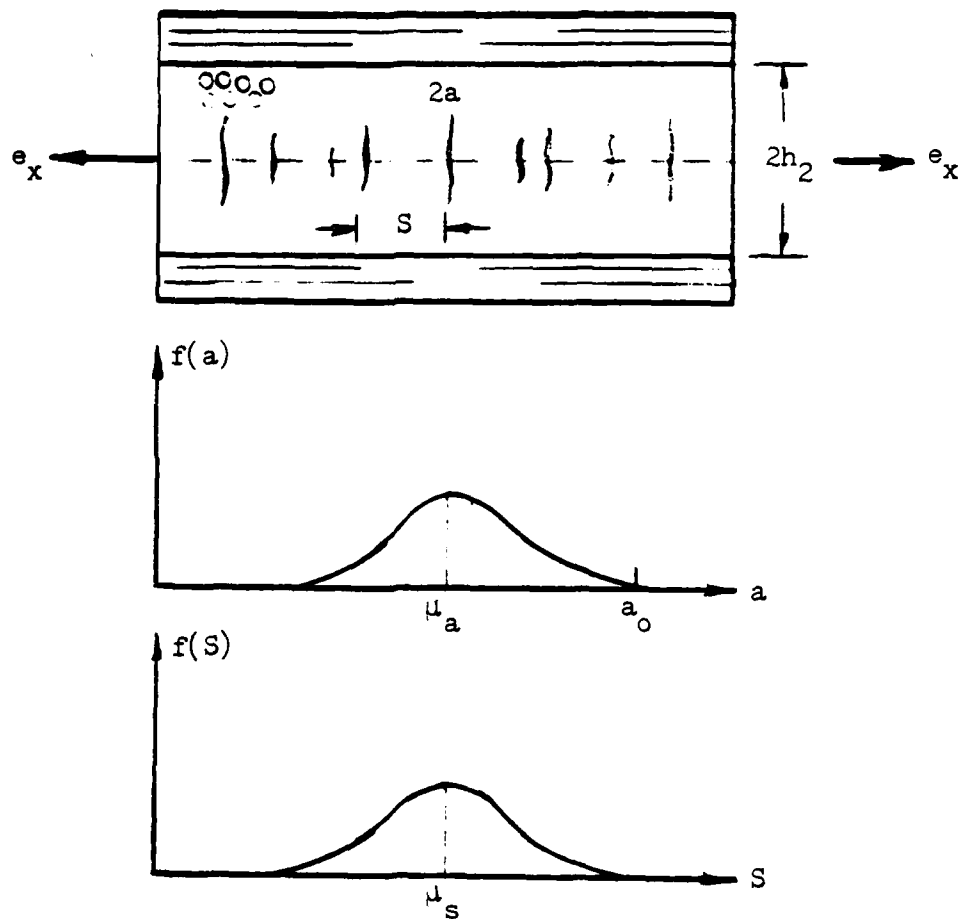


Fig. 8 Effective Flaws in 90° Layer(top); Size a and Spacing S Distributions(below).

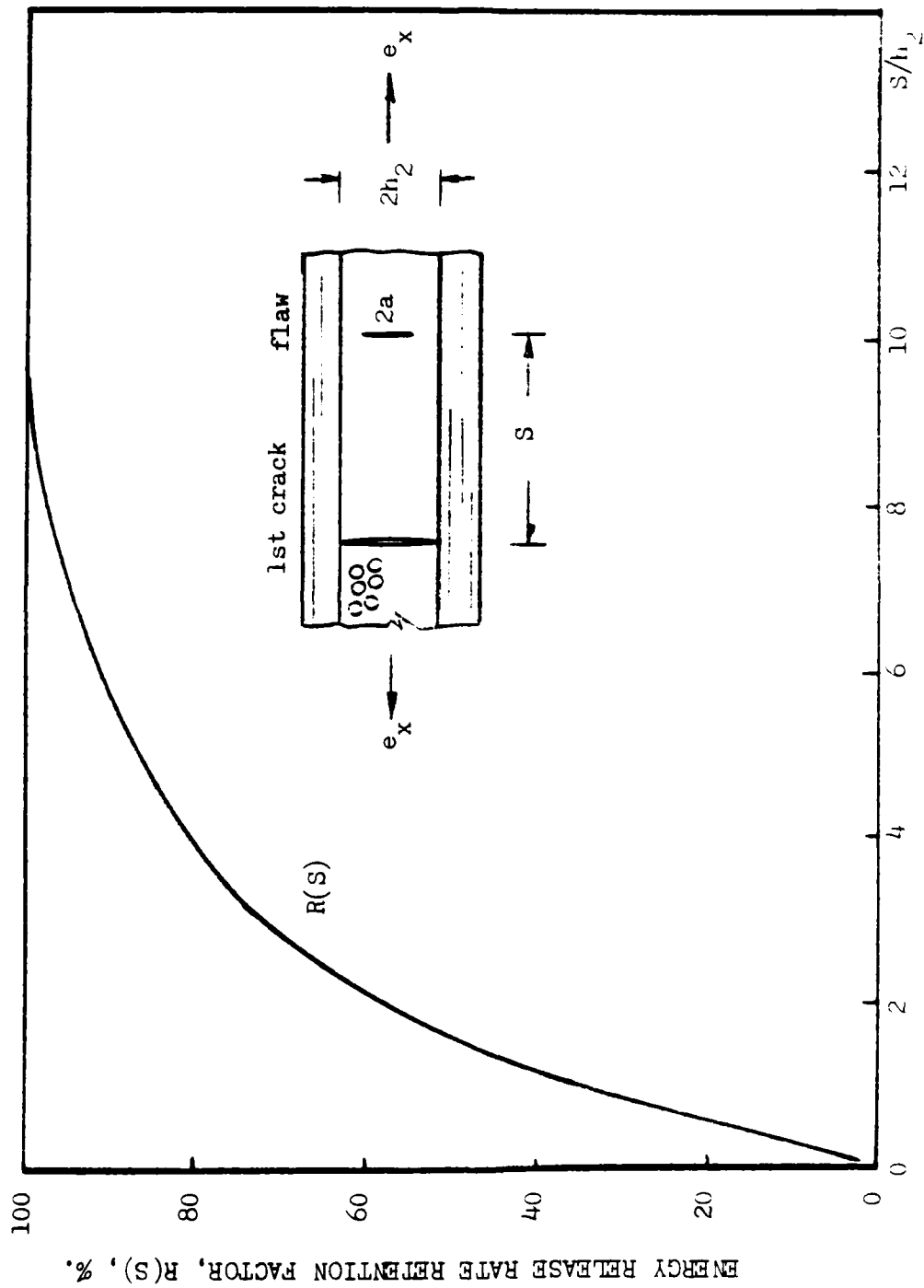


Fig. 9 Energy Release Rate Retention Factor $R(S)$ for a Flaw Located at a Distance S from a Transverse Crack.

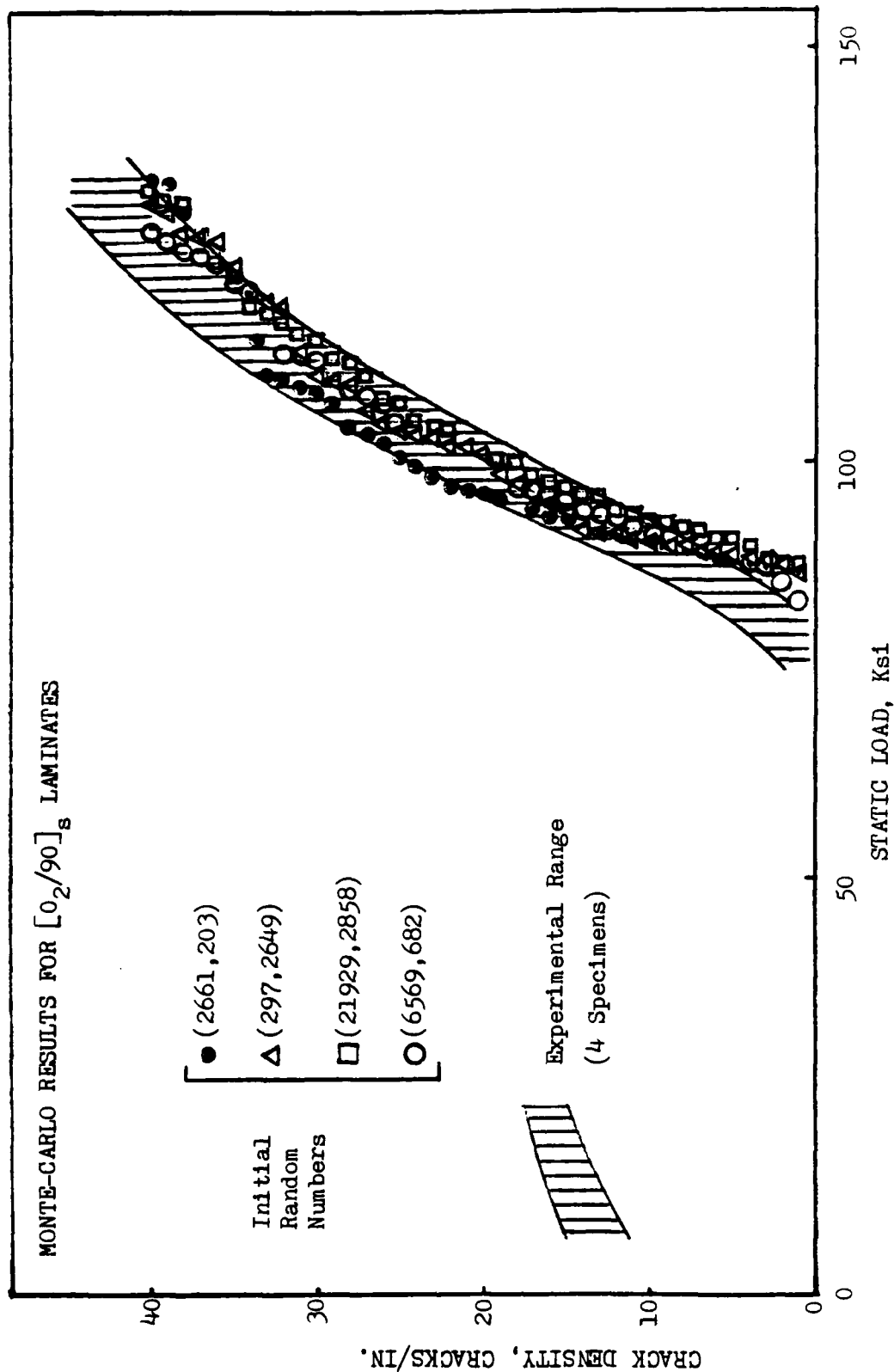


Fig. 10 Comparison of Experiment and the Monte-Carlo simulations of Transverse Cracks.

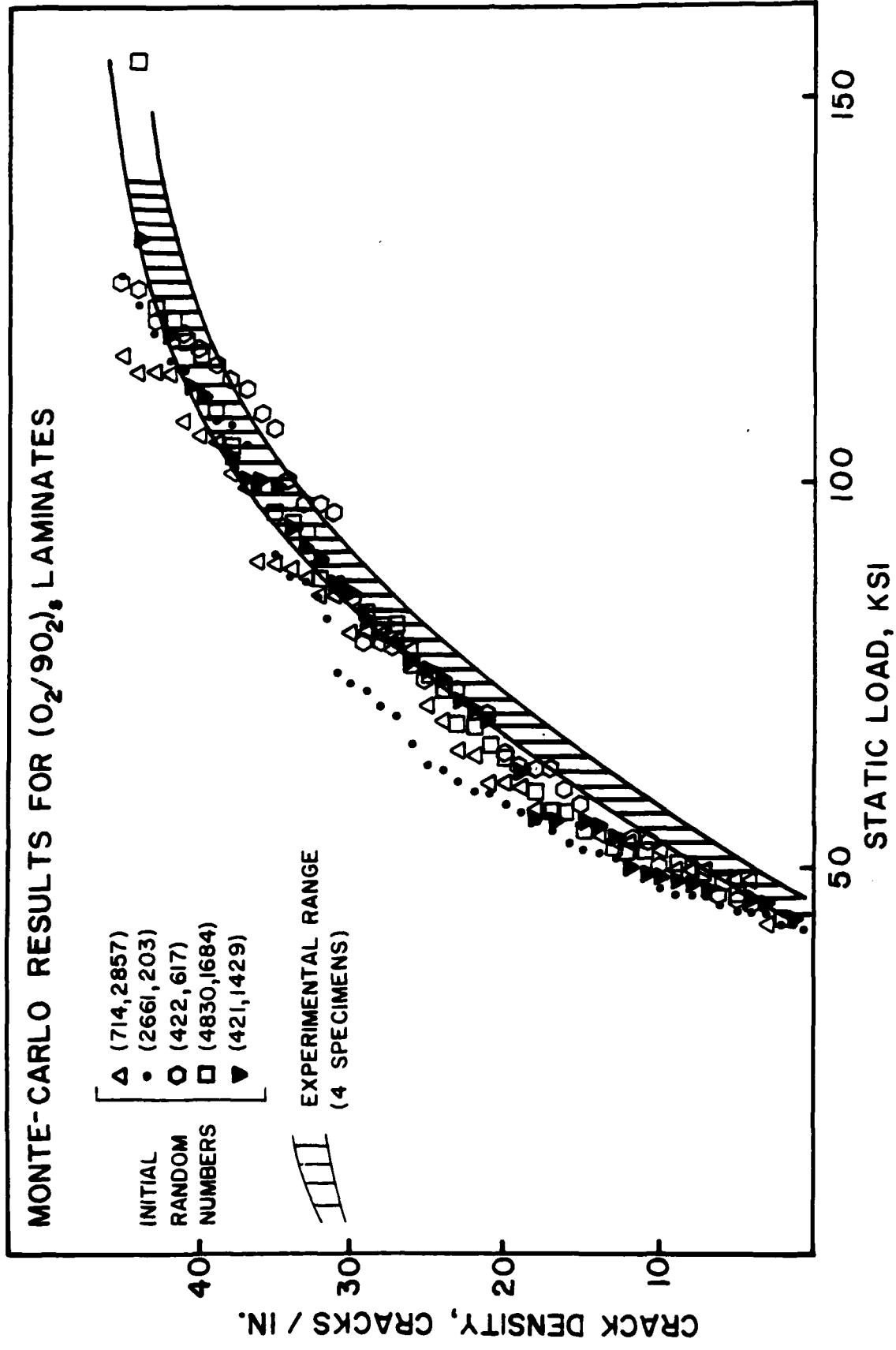


Fig. 11 Comparison of Experiment and the Monte-Carlo Simulations of Transverse Cracks.

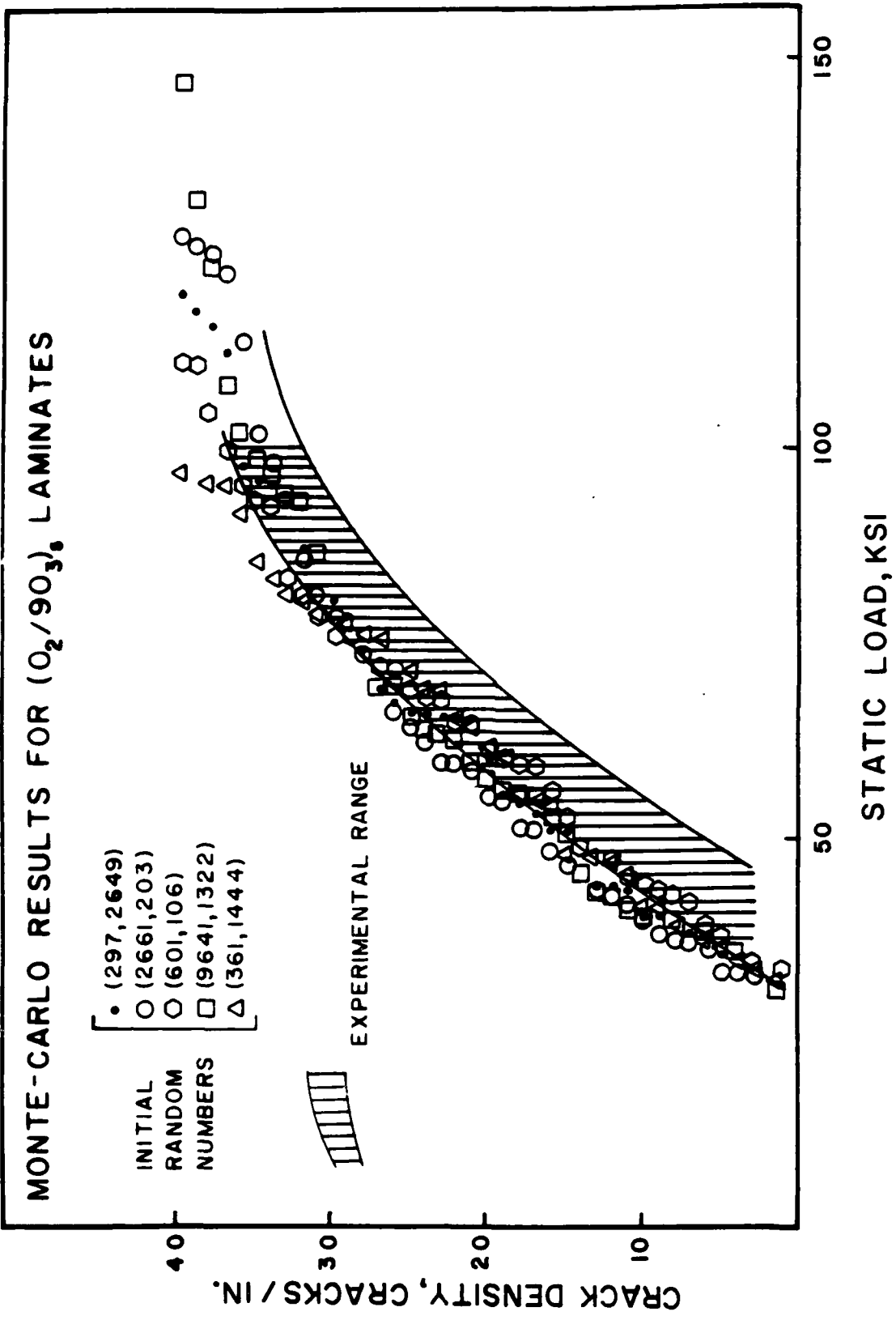
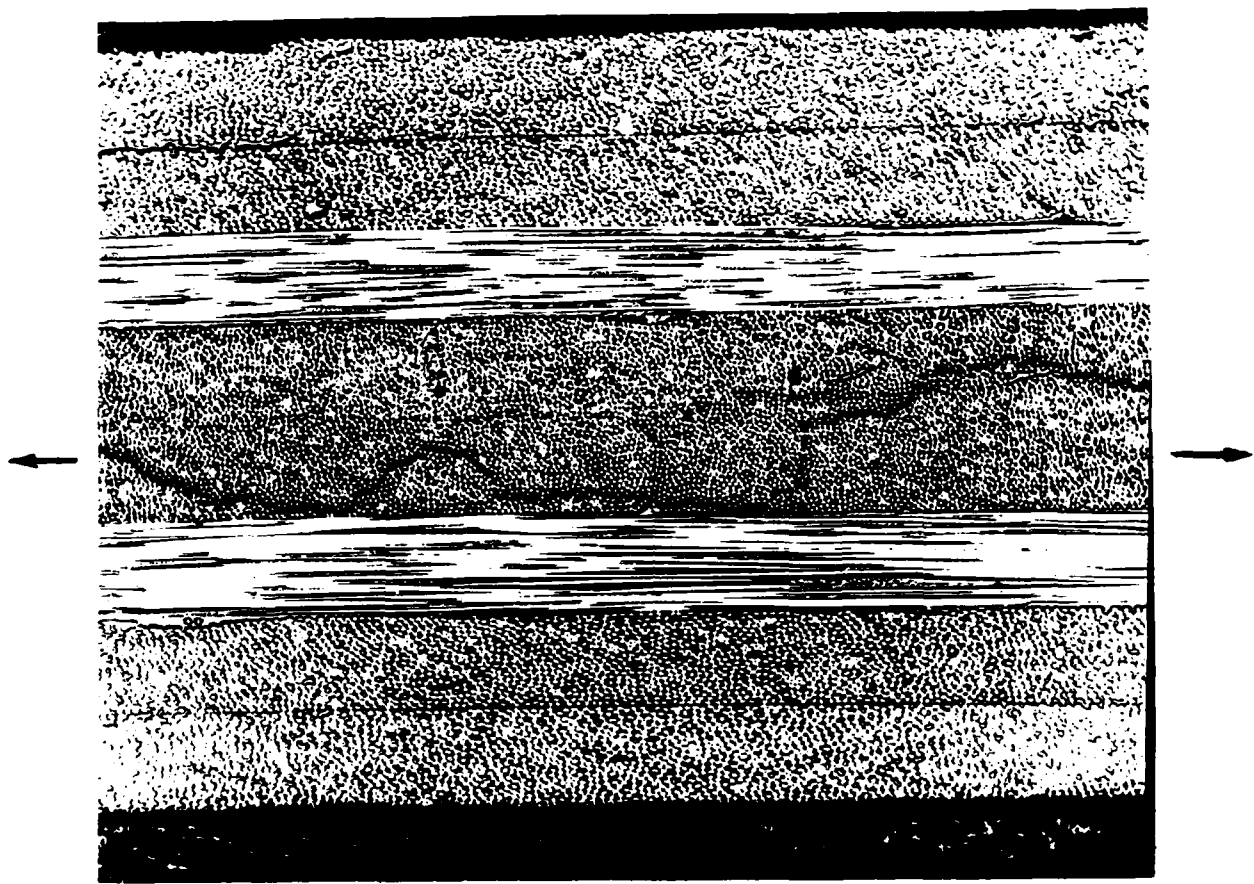


Fig. 12 Comparison of Experiment and the Monte-Carlo Simulations of Transverse Cracks.



VIEW AT
RIGHT
80X

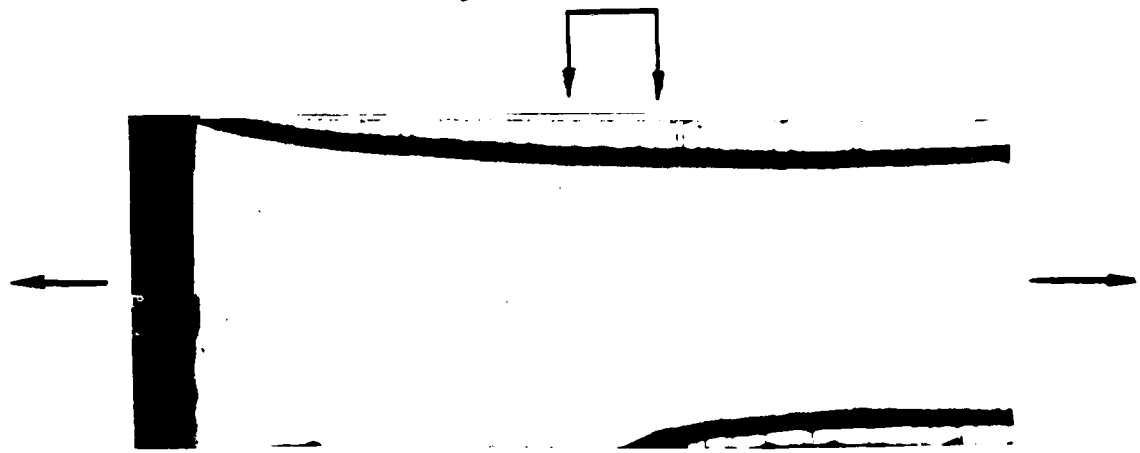


Fig. 10. Shear deformation in a $[+45/0/90]_3$ laminate.

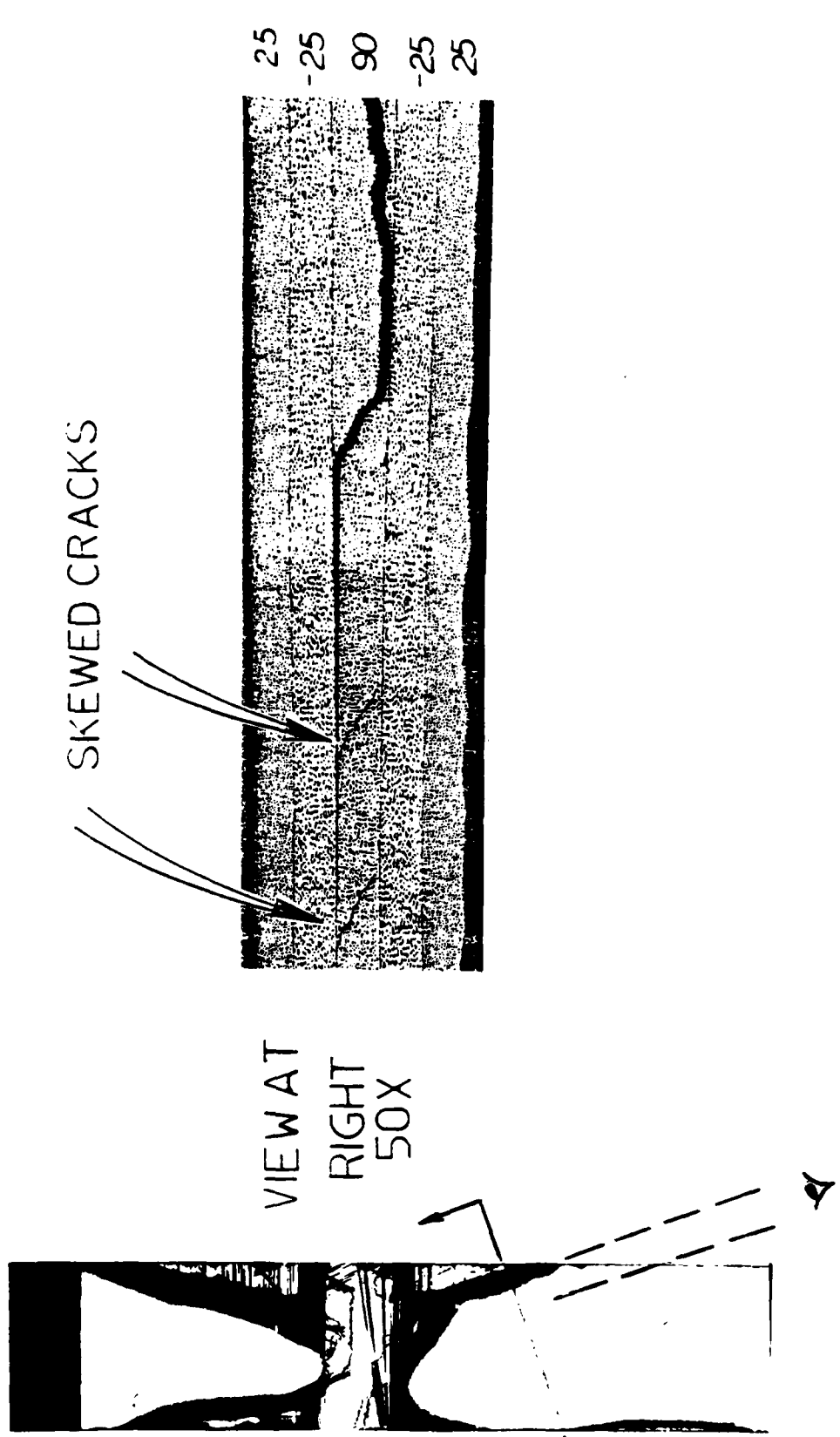


Fig. 14 Microphotograph(right) Showing Free Edge Delamination of a $[+25/90]_{1/2}$ s Laminate After Final Failure. Note Skewed Cracks Ahead of Delamination.

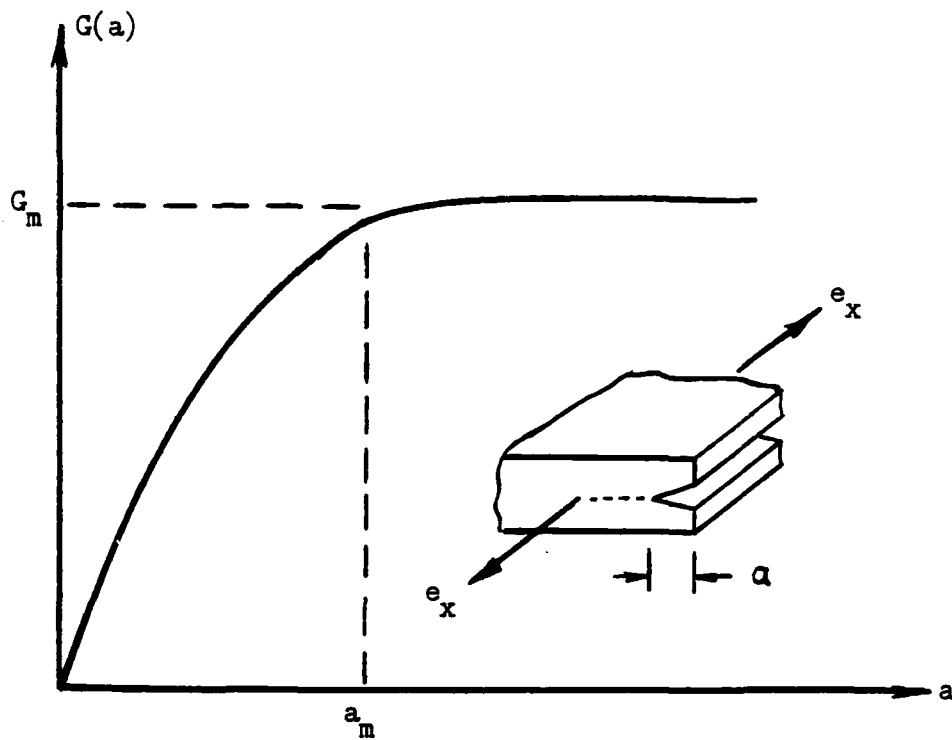


Fig. 15 Typical Shape of Energy Release Rate $G(a)$ for Delamination.

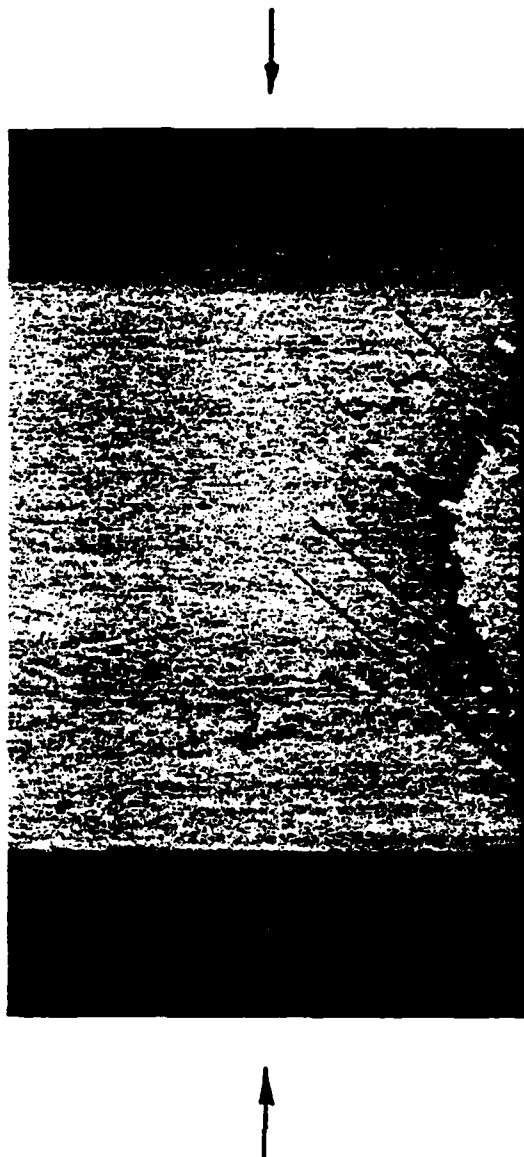
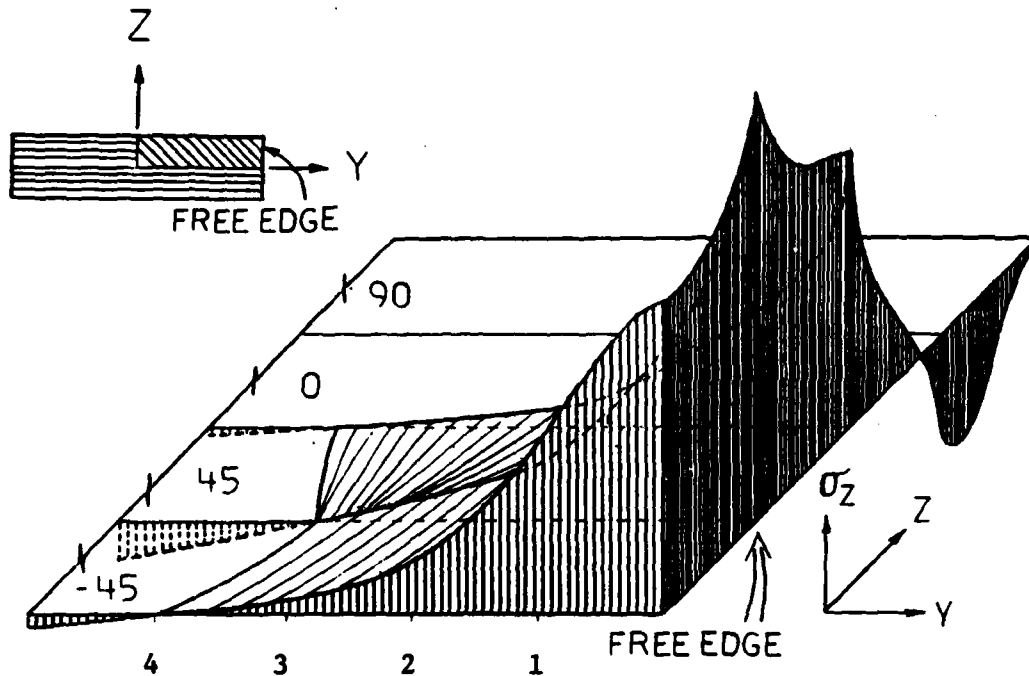


Fig. 16 Free Edge Delamination Induced by Compression.
AS-3501-06 $[90_2/0_2/\pm 45_2]_s$.



Interlaminar Normal Stress Distribution

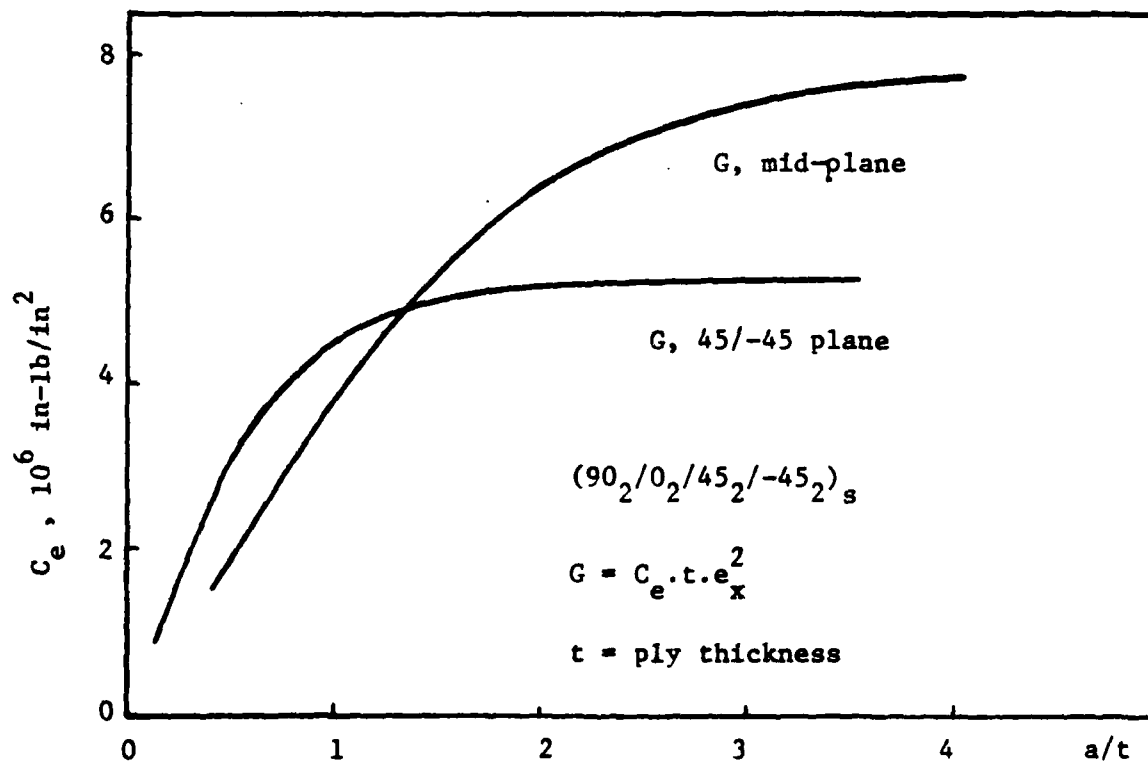
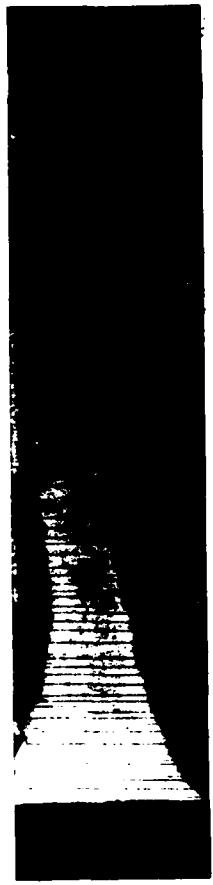


Figure 17 Interlaminar Normal Stress Distribution and Energy Release Rate Coefficients for $(90_2/0_2/\pm 45_2)_s$ Under Compression.



a



b

Fig. 18 (a) Delamination Induces Transverse Cracks, $[\pm 25/90_2]_S$;
(b) Transverse Cracks induce Delaminations, $[\pm 25/90_4]_S$.

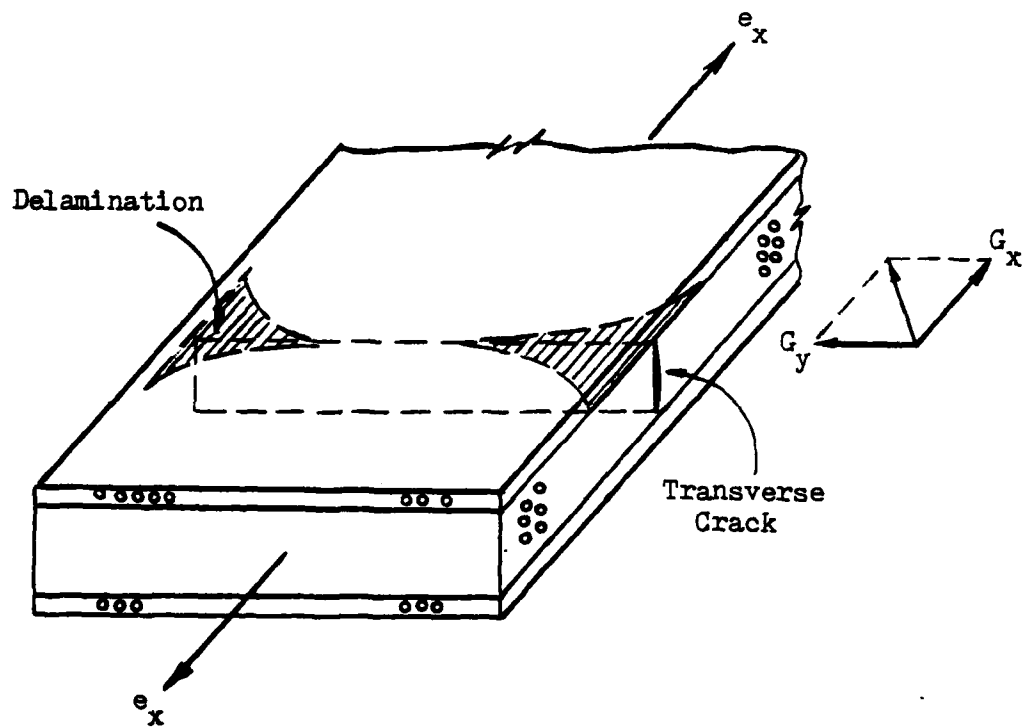


Fig. 19 Transverse Crack/Delamination Interaction.

CASE STUDY Transverse cracking/Delamination/Final failure Sequence.

T300/934 $(\pm 25/90_n)_s$, $n=1/2, 1, 2, 3, 4, 6, 8$.

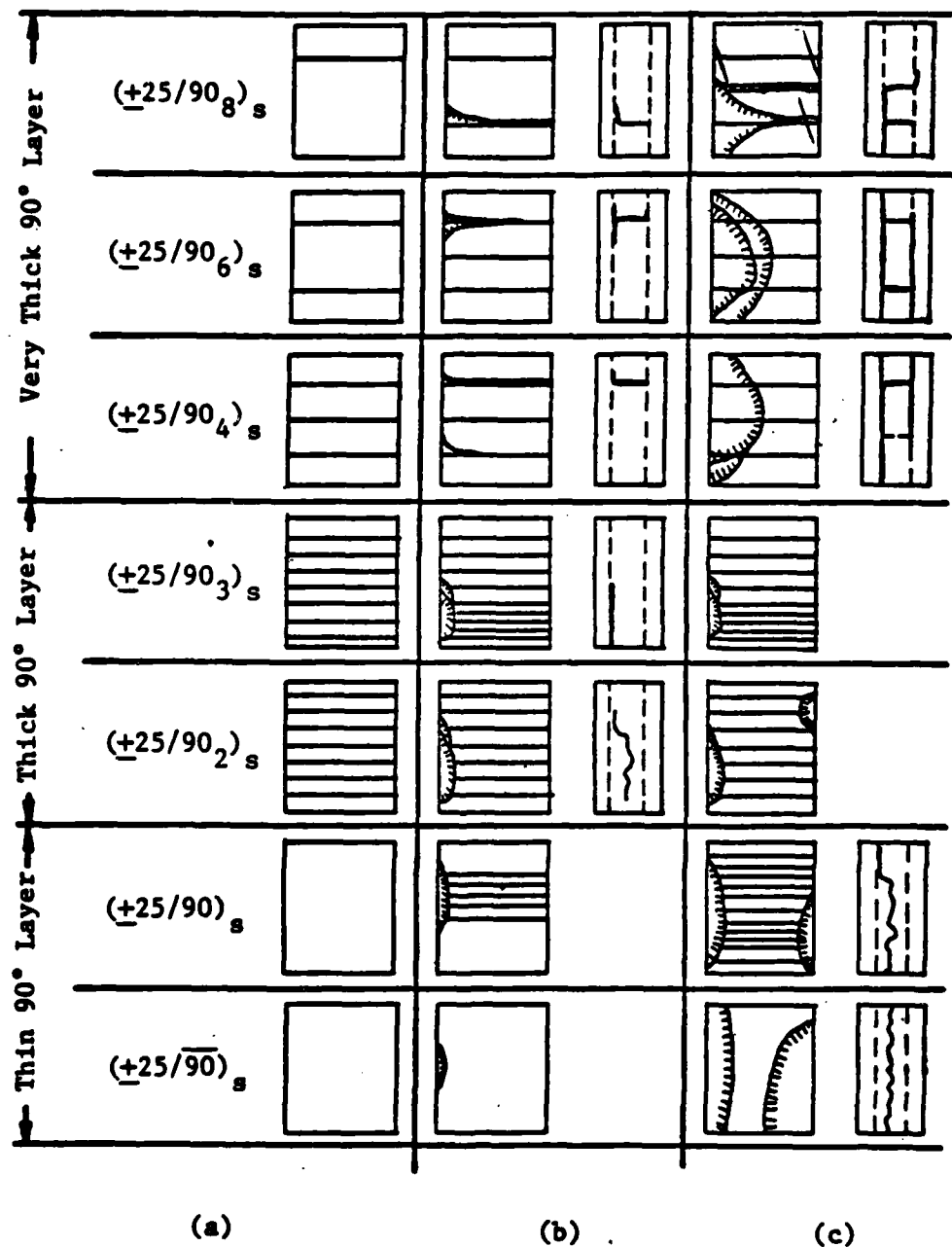
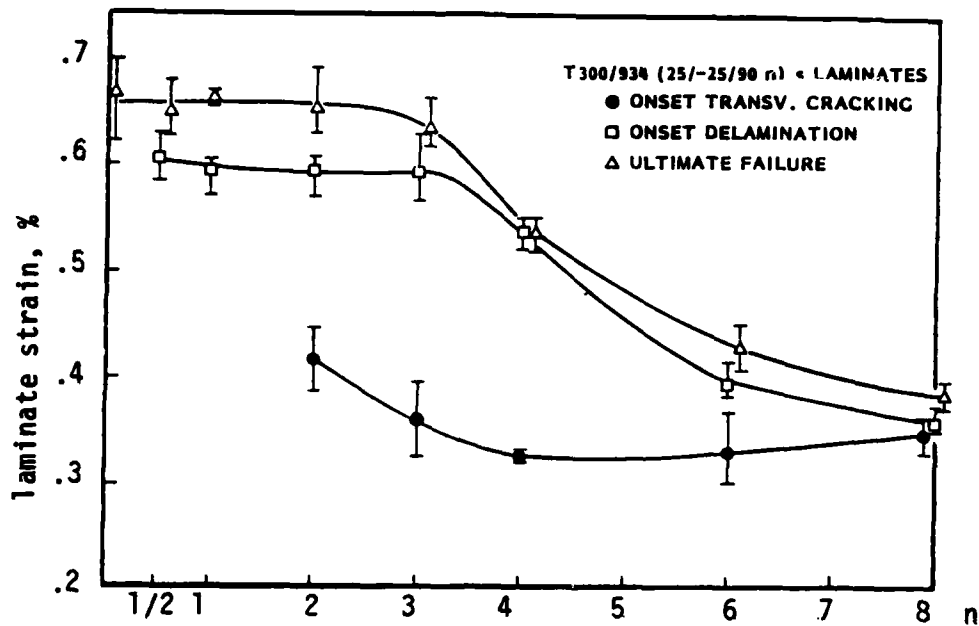
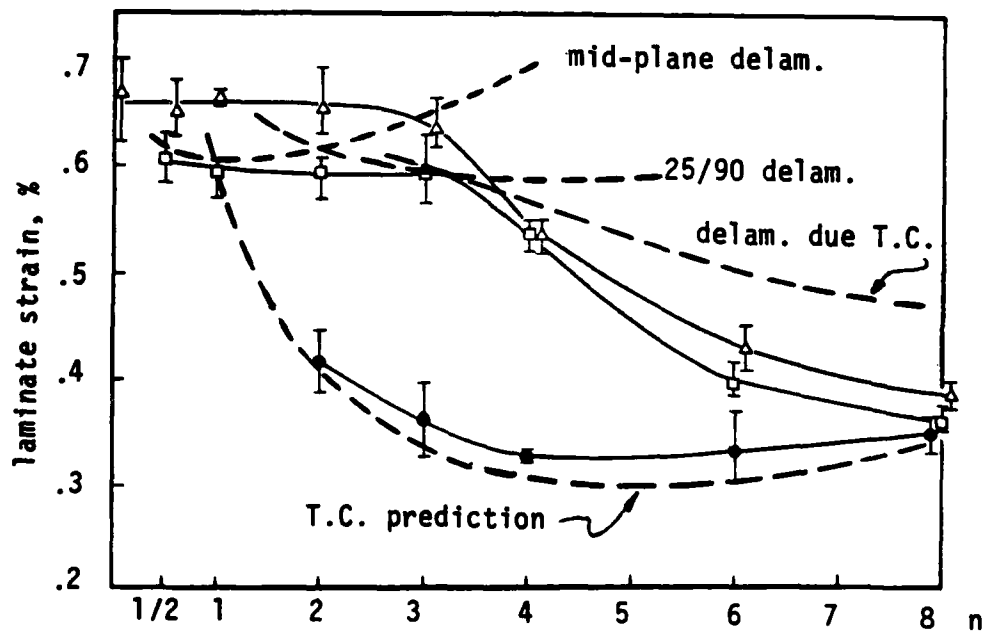


Fig. 20 SCHEMATIC OF THE FRACTURE SEQUENCE IN THE $(\pm 25/90_n)_s$ LAMINATES
 (a) JUST PRIOR TO EDGE DELAMINATION, (b) SUBSEQUENT TO EDGE
 DELAMINATION, (c) JUST PRIOR TO FINAL FAILURE



(a) Experimental Results



(b) Comparison with Predicted Results

Fig. 21 Onset Loads at Transverse Crack, Edge Delamination and Final Failure for the $[\pm 25/90]_n$ Laminate Series.

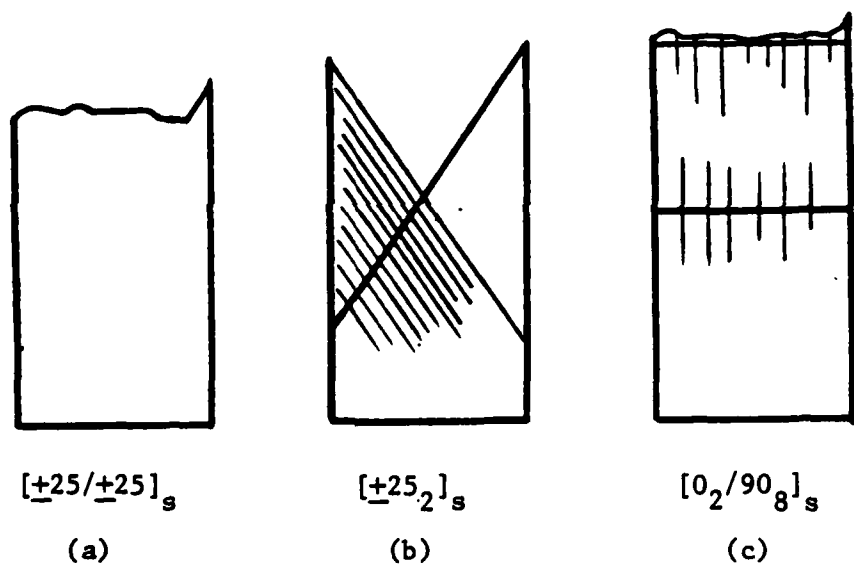


Figure 22 Final Failure Modes: (a) Cross-sectional Fiber Break; (b) 25-layer Transverse Cracks; (c) 0-layer Fiber Splits over 90-layer Transverse Cracks.

REFERENCES

- [1] Tsai, S. W. and Hahn, H. T., "Introduction to Composite Materials," Technomics, 1980.
- [2] Starnes, J. H. and Rouse, M., "Post-Buckling and Failure Characteristics of Selected Flat Rectangular Graphite-Epoxy Plates Loaded in Compression," Proc. AIAA/ASME/ASCE/AHS, 22nd Structures, Structural Dynamics and Materials Conference, 1981.
- [3] Starnes, J. H. and Williams, J. G., "Failure Characteristics of Graphite-Epoxy Structural Components Loaded in Compression," NASA-TR-84552, 1982.
- [4] Waddoups, M. E., Eisenmann, J. R. and Kaminski, B. E., "Macroscopic Fracture Mechanics of Advanced Composite Materials," J. Comp. Matls., Vol. 5, 1971, p. 466.
- [5] Cruse, T. A., "Tensile Strength of Notched Composites," J. Comp. Matls., Vol. 7, 1973, p. 218.
- [6] Whitney, J. M. and Nuismer, R. J., "Stress Fracture Criteria for Laminated Composites Containing Stress Concentrations," J. Comp. Matls., Vol. 8, 1974, p. 253.
- [7] Cooper, G. A. and Kelly, A., "Role of the Interface in the Fracture of Fiber-Composite Materials," ASTM STP 452, 1969, p. 90.
- [8] Greszczuk, L. B., "Theoretical Studies of the Mechanisms of the Fiber-Matrix Interface in Composites," ASTM STP 452, 1969, p. 42.
- [9] Kelly, A., "Interface Effects and the Work of Fracture of a Fibrous Composites," Proc. Roy. Soc., A319, 1970, p. 95.
- [10] Phillips, D. C. and Tetelman, A. S., "The Fracture Toughness of Fiber Composites," Composites, Vol. 3, 1972, p. 216.
- [11] Piggott, M. R., "Theoretical Estimation of Fracture Toughness of Fibrous Composites," J. Matl. Sci., Vol. 5, 1970, p. 669.
- [12] Zweben, C. and Rosen, B. W., "A Statistical Theory of Material Strength with Application to Composite Materials," J. Mech. Phys. Solids, Vol. 18, 1970, p. 189.
- [13] Corten, H. T., "Fracture Mechanics of Composites," Fracture, Vol. 7, Ed. H. Liebowitz, Academic Press, N.Y., 1972, p. 676.
- [14] Wu, E. M., "Application of Fracture Mechanics to Anisotropic Plates," J. Appl. Mech., Vol. 34, 1967, p. 967.

- [15] Kanninen, M. F., Rybicki, E. F. and Brinson, H. F., "A Critical Look at Current Applications of Fracture Mechanics to the Failure of Fiber-Reinforced Composites," Composites, Vol. 8, 1977, p. 17.
- [16] Wang, A. S. D., Crossman, F. W. and Law, G. E., "Interlaminar Failure in Epoxy-Based Composite Laminates," Proc. 29th MFPG Symp. Advance Composites-Design and Applications, NBS, 1979, p. 255.
- [17] Wang, A. S. D. and Law, G. E., "An Energy Method for Multiple Transverse Cracks in Graphite-Epoxy Laminates," in Modern Dev. in Composite Materials and Structures, Ed. J. Vinson, ASME, 1979, p. 17.
- [18] Wang, A. S. D. and Crossman, F. W., "Initiation and Growth of Transverse Cracks and Edge Delamination in Composite Laminates: Part I. An Energy Method," J. Comp. Mats., Suppl. Vol., 1980, p. 71.
- [19] Crossman, F. W., Warren, W. T., Wang, A. S. D. and Law, G. E., "Initiation and Growth of Transverse Cracks and edge delamination in Composite Laminates: Part 2. Experimental Correlation," J. Comp. Mats., Suppl. Vol., 1980, p. 88.
- [20] Wang, A. S. D., "Growth Mechanisms of Transverse Cracks and Ply-Delamination in Composite Laminates," Proc. ICCM-III, Vol. 1, Paris, 1980, p. 170.
- [21] Crossman, F. W. and Wang, A. S. D., "The Dependence of Transverse Cracks and Delamination on Ply Thickness in Graphite-Epoxy Laminates," ASTM STP 725, 1982, p. 170.
- [22] Wang, A. S. D., Miller, H. R. and Chou, P. C., "A Theory for Multiple Transverse Cracks in Composite Laminates," in Advances in Aerospace Structures and Materials, Ed. J. Vinson, ASME, 1982, p. 51.
- [23] Griffith, A. A., "The Phenomena of Rupture and Flow in Solids," Phil. Trans. Roy Soc., Vol. A221, 1920, p. 163.
- [24] Irwin, G. R., "Fracture Dynamics," in Fracture of Metals, ASM, Cleveland, 1948, p. 147.
- [25] Orowan, E. O., "Fundamentals of Brittle Behavior of Metals," in Fatigue and Fracture of Metals, W. M. Murray, Ed. Wiley & Sons, N.Y., 1950, p. 139.
- [26] Muskhelishvili, N. I., "Some Basic Problems From the Mathematical Theory of Elasticity," Noordhoff, Holland, 1953.
- [27] Sneddon, I. N., "Integral Transform Methods," in Methods of Analysis and Solutions of Crack Problems, Noordhoff, Holland, 1973, p. 315.
- [28] Lekhnitsky, S. G., "Theory of Elasticity of an Anisotropic Elastic Body," Holden-Day, San Francisco, 1963.

- [29] Rice, J. R., "A Path in Dependent Integral and Approximate Analysis of Strain Concentration by Notches and Cracks," J. Appl. Mech. Trans. ASME, 1968, p. 379.
- [30] Bucci, R. J., Paris, P. C., Landis, J. D. and Rice, J. R., "J-Integral Estimation Procedures," in Fracture Toughness, ASTM STP 514, 1972, p.40.
- [31] Irwin, G. R., "Fracture," Handbuch der Physik, Vol. 5, Springer-Verlag, 1958, p. 551.
- [32] Rybicki, E. F. and Kanninen, M. F., "A Finite Element Calculation of Stress Intensity Factors by a Modified Crack-Closure Integral," Eng. Fract. Mech., Vol. 9, 1977, p. 931.
- [33] Wang, A. S. D. and Crossman, F. W., "Some New Results on Edge Effects in Symmetric Composite Laminates," J. Comp. Matls., Vol. 11, 1977, p. 92.
- [34] Raju, I. S. and Crews, J. H., "Three Dimensional Analysis of [0/90] and [90/0] Laminates With a Central Circular Hole," Composites Tech. Rev., Vol. 4, 1982, p. 116.
- [35] Spilker, R. L., and Chou, S. C., "Edge Effects in Symmetric Composite Laminates: Importance of Satisfying the Traction Free Edge Condition," J. Comp. Matls., Vol. 14, 1980, p.2.
- [36] Wang, S. S. and Choi, I., "Boundary Layer Effects in Composite Laminates," Part 1 and Part 2, J. Appl. Mech., Vol. 49, 1982, p. 541, p. 549.
- [37] Isida, M., "Method of Laurant Series Expansion for Internal Crack Problems," in Methods of Analysis and Solutions of Crack Problems, Ed. G. C. Sih, Noordhoff, 1973, p. 56.
- [38] Whitcomb, J. D., Raju, I. S. and Goree, J. G., "Reliability of the Finite Element Method for Calculating Free Edge Stresses in Composite Laminates," Computers & Structures, Vol. 15, 1982, p. 23.
- [39] Cullen, J. S., "Mode-I Delamination of Unidirectional Graphite Epoxy Composite Under Complex Load Histories," M. S. Theses, Texas A & M Univeristy, 1981.
- [40] Williams, D., "Mode-I Transverse Cracking in an Epoxy and a Graphite Fiber Reinforced Epoxy," M. S. Thesis, Texas A & M University, 1981.
- [41] Wilkins, D. J., "A Comparison of the Delamination and Environmental Resistance of a Graphite-Epoxy and a Graphite-Bismaleimide," NAV-GD-0037, Naval Air System Comm., 1981.
- [42] Wilkins, D. J., Eisenmann, J. R., Camin, R. A., Margolis, W. S. and Benson, R. A., "Characterizing Delamination Growth in Graphite-Epoxy," ASTM STP 775, 1982, p. 168.

- [43] Vanderkley, P. S., "Mode-I and Mode-II Delamination Fracture Toughness of an Unidirectional Graphite-Epoxy Composite," M. S. Thesis, Texas A & M University, 1981.
- [44] Bascom, W. D., Cottington, R. L. and Timmons, C. O., "Fracture Design Criteria for Structural Adhesive Bonding - Promise and Problems," Naval Eng. Jour., Aug. 1976, p. 73.
- [45] Wang, A. S. D., Kishore, N. N. and Feng, W. W., "On Mixed-Mode Fracture in Off-Axis Unidirectional Graphite-Epoxy Composites," Proc. ICCM-IV, Vol. 1, Tokyo, 1982, p. 599.
- [46] Bader, M. G., Bailey, J. E., Curtis, P. T. and Parvizi, A., "The Mechanisms of Initiation of Development of Damage in Multi-Axial Fiber-Reinforced Plastics Laminates," in Mechanical Behavior of Materials, ICM-3, Vol. 3, 1979, p. 227.
- [47] Aveston, J. and Kelly, A., "Theory of Multiple Fracture of Fibrous Composites," J. Matls. Sciences, Vol. 8, 1973, p. 352.
- [48] Reifsnider, K. L. and Masters, J. L., "Investigation of Characteristic Damage States in Composites Laminates," ASME Paper No. 78-WA-AERO-4, 1978.
- [49] Chou, S. C., Brockelman, R., Broz, A., Hinton, Y. and Shuford, R., "Analytical and NDE Techniques for Determining Crack Initiation in Graphite-Epoxy Laminates," ASTM Symp. Effects of Defects in Composite Materials, San Francisco, 1982.
- [50] Juvinall, R. C., "Stress, Strain and Strength," McGraw Hill, N.Y., 1967, p. 346.
- [51] Wang, A. S. D. and Lei, C. S., "Multiple Transverse Cracks by a Monte-Carlo Simulation," (in press).
- [52] Chou, P. C., Wang, A. S. D. and Miller, H. R., "Cumulative Damage Model for Advanced Composite Materials," AFWAL-TR-82-4083, U. S. Air Force Wright Aeronautical Lab., 1982.
- [53] Pipes, R. B. and Pagano, N. J., "Interlaminar Stresses in Composite Laminates Under Uniform Axial Tension," J. Comp. Matls, Vol. 4, 1970, p. 538.
- [54] Bjeletich, J. G., Crossman, F. W. and Warren, W. J., "The Influence of Stacking Sequence on Failure Modes in Quasi-Isotropic Graphite-Epoxy Laminates," Failure Modes in Composites - IV. AIME, 1979.
- [55] Rodini, B. T. and Eisenmann, J. R., "An Analytical and Experimental Investigation of Edge Delamination in Composite Laminates," in Fibrous Composites in Structural Design, Ed. E. M. Leno, et. al., Pleum Press, N.Y., 1978, p. 441.

- [56] Law, G. E., "Fracture Analysis of [+25/90_n] Graphite-Epoxy Composite Laminates," Ph.D. Thesis, Drexel University, 1981.
- [57] Wang, A. S. D. and Slomiana, M., "Fracture Mechanics of Delamination - Initiation and Growth," NADC-TR-79056-60, 1982.
- [58] Crossman, F. W., "Experimental Documentation of the Sequential Failure Modes in Graphite-Epoxy Laminates," (in press).

END

FILMED

4-84

DTIC